Proxy-Model Comparison for the Eocene-Oligocene Transition in Southern High Latitudes

Emily Tibbett[1], Natalie J Burls[2], David Hutchinson[3], and Sarah J Feakins[1]

[1]University of Southern California
[2]George Mason University
[3]University of New South Wales

December 16, 2022

Abstract

The Eocene-Oligocene Transition (EOT) marks the shift from greenhouse to icehouse conditions at 34 Ma, when a permanent ice sheet developed on Antarctica. Climate modeling studies have recently assessed the drivers of the transition globally. Here we revisit those experiments for a detailed study of the southern high latitudes in comparison to the growing number of mean annual sea surface temperature (SST) and mean air temperature (MAT) proxy reconstructions, allowing us to assess proxy-model temperature agreement and refine estimates for the magnitude of the $p\mathrm{CO_2}$ forcing of the EOT. We compile and update published proxy temperature records on and around Antarctica for the late Eocene (38-34 Ma) and early Oligocene (34-30 Ma). Compiled SST proxies cool by up to 3°C and MAT by up to 4°C between the timeslices. Proxy data were compared to previous climate model simulations representing pre- and post-EOT, typically forced with a halving of $p\mathrm{CO_2}$. We scaled the model outputs to identify the magnitude of $p\mathrm{CO_2}$ change needed to drive a commensurate change in temperature to best fit the temperature proxies. The multi-model ensemble needs a 30 or 33% decrease in $p\mathrm{CO_2}$, to best fit MAT or SST proxies respectively, a difference of just 3%. These proxy-model intercomparisons identify $p\mathrm{CO_2}$ as the primary forcing of EOT cooling, with a magnitude (-200 or -243 ppmv) approaching that of the $p\mathrm{CO_2}$ proxies (-150 ppmv). However individual model estimates span -66 to -375 ppmv, thus proxy-model uncertainties are dominated by model divergence.

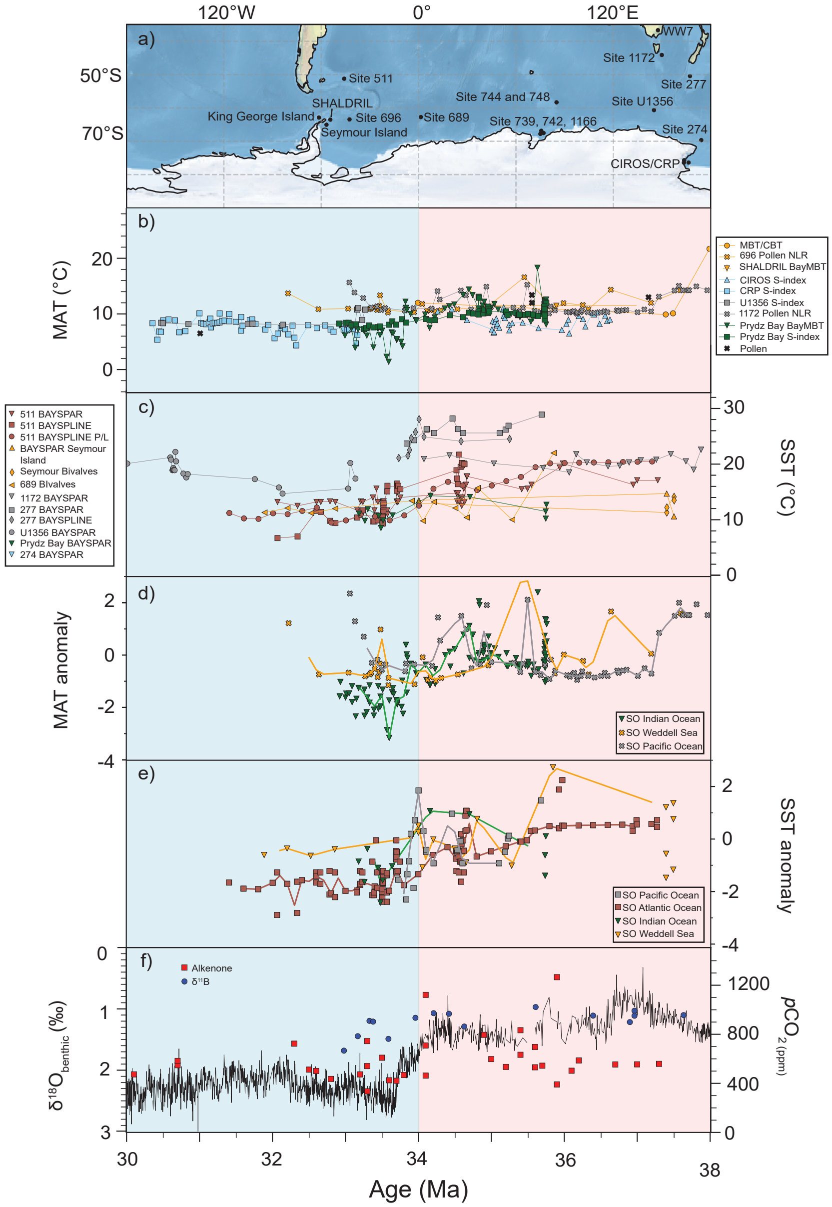

Figure 1: Proxy data compiled for Antarctica, the Southern Ocean and the southern high latitudes spanning the Eocene and Oligocene. a) Map depicting location of records used in this study. b) Land surface mean air temperature (MAT) data including BayMBT (Tibbett et al., 2021a, 2022b), pollen climate reconstructions including NLR (Amoo et al., 2022; Francis et al., 2008; Macphail & Truswell, 2004; Passchier et al., 2013; Poole et al., 2005; Thompson et al., 2022; Truswell & Macphail, 2009), S-index (Passchier et al., 2013, 2017), and MBT/CBT (Douglas et al., 2014). c) Sea surface temperature (SST) data from BAYSPAR calibrated TEX86 data (Douglas et al., 2014; Hartman et al., 2018; Houben et al., 2019; Lauretano et al., 2021; Pagani et al., 2011), SSTs from BAYSPLINE calibrated Uk'37 (Houben et al., 2019; Liu et al., 2009; Pagani et al., 2011; Plancq et al., 2014), and Δ47 from bivalves (Douglas et al., 2014; Petersen & Schrag, 2015). d) Air Temperature anomaly and e) sea surface temperature anomaly for each Southern Ocean sector with data normalized by the respective datasets Eocene mean in standard deviation units (Z scores), combined for each Southern Ocean sector, and then interpolated to a common interval with a spline fit to the data. Only datasets covering the late Eocene and early Oligocene were used for the temperature anomaly plot. f) δ18Obenthic spline (Westerhold et al., 2020) and pCO2 compiled from δ11B (blue) and alkenone (red) proxies (Rae et al., 2021).

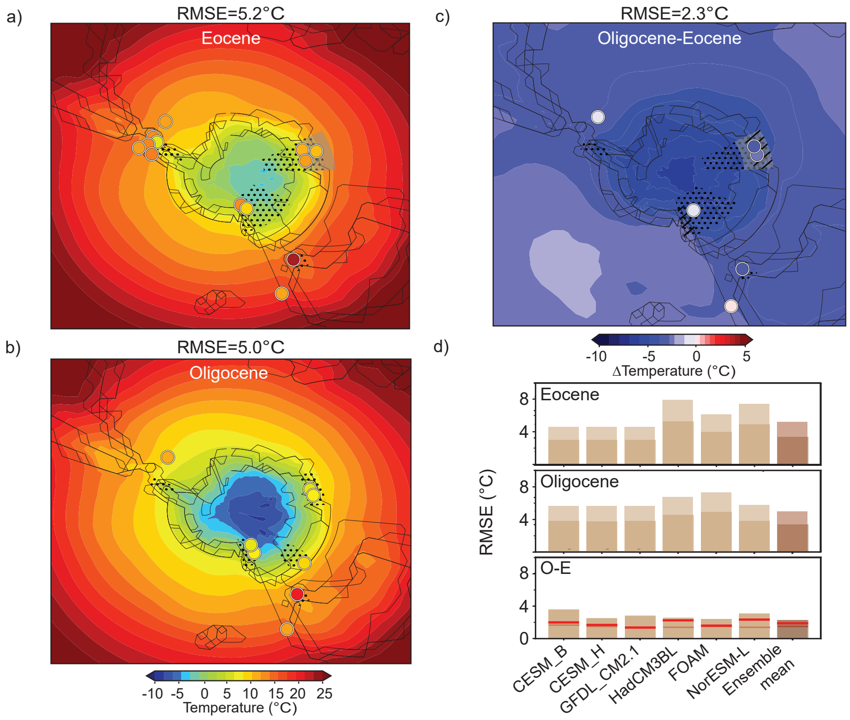

Figure 2: Southern hemisphere model MAT for the a) Eocene (4x pCO2), b) Oligocene (2x pCO2 model runs), and c) the difference across the transition (2x-4x) showing results for the unscaled multi model ensemble mean. The circles correspond to proxy mean annual air temperature records while the dotted areas show the source area used to compare the model temperature to the proxy record. d) The RMSE for pCO2 model runs for MAT, for individual model mapped output see Figure S1. Red lines are the RMSE for each model after the pCO2 scaling for RMSE values see Table S1.

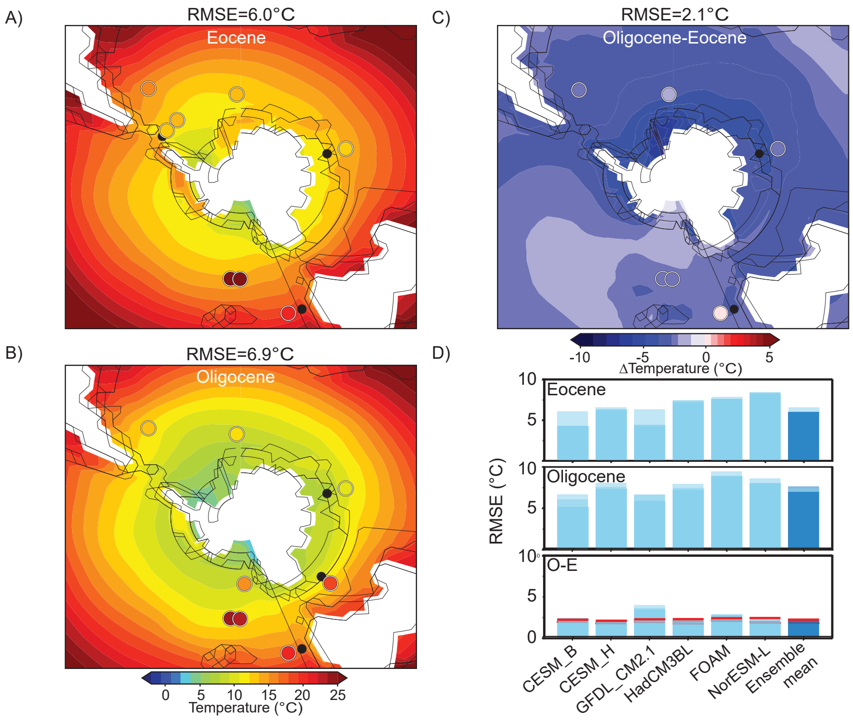

Figure 3: Southern Ocean sea surface temperatures (SST) for the a) Eocene (4x pCO2), b) Oligocene (2x pCO2 model runs), and c) the difference across the transition (2x-4x) showing results for the unscaled multi model ensemble mean. The circles correspond to proxy mean annual air temperature records while the dotted areas show the source area used to compare the model temperature to the proxy record. d) Summarizing the RMSE for pCO2 model runs for SST, for individual model mapped output see Figure S3. Red lines are the RMSE for each model after the pCO2 scaling for RMSE values see Table S1.

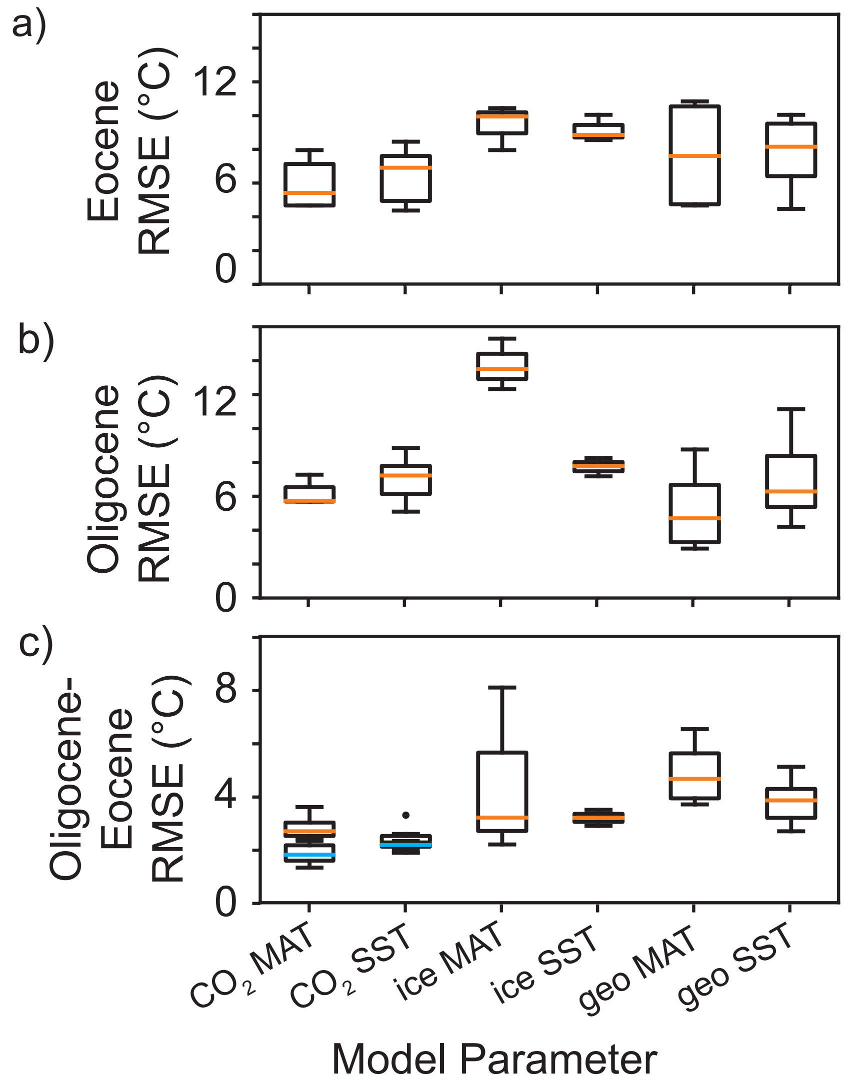

Figure 4: Summary of average RMSE across the model experiments a) Eocene runs for CO2 using 4x pCO2 (Table 3), ice runs contain no ice with pCO2 of 560 ppmv, Eocene paleogeography runs (Table 3) b) Oligocene runs for pCO2 using 2x pCO2, ice runs containing the model prescribed ice sheet with pCO2 of 560 ppmv, and Oligocene paleogeography runs c) is the difference model outputs between the Oligocene and Eocene runs. (Table 3). The x axis headers correspond as follows: CO2 distinguishes the proxy-model comparison based on pCO2 changes, ice for the with and without an ice sheet, and geo for the model runs with paleogeographic changes. MAT and SST correspond to either air or sea surface temperature comparison Mean is the orange line with outliers as dots. Dots are outliers with both from the GFDL CM2.1 model. Blue line is the ensemble mean from the pCO2 scaling.

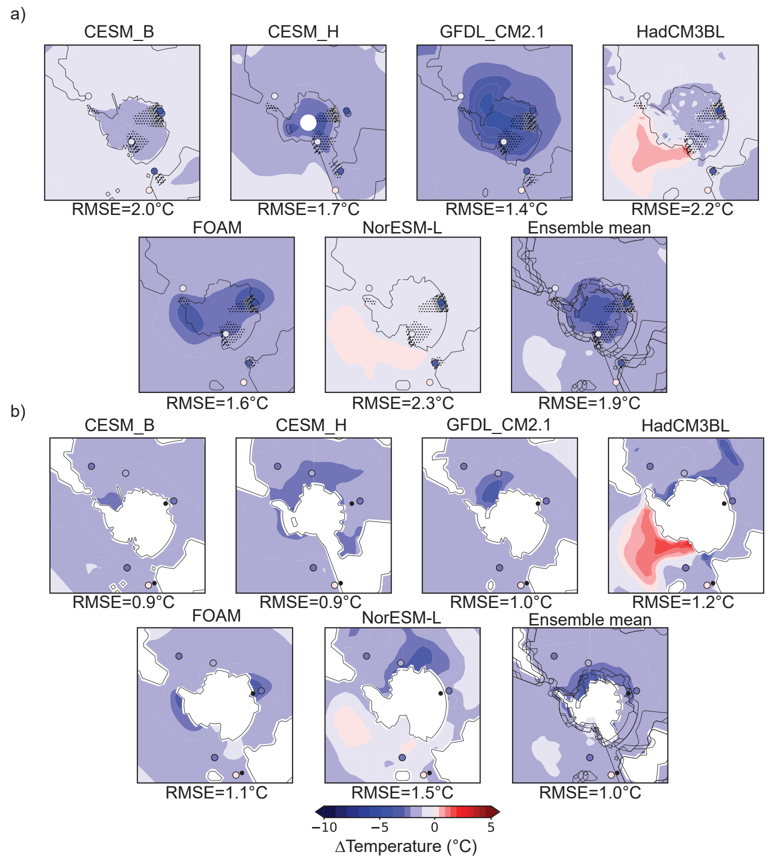

Figure 5: Proxy-model [?]MAT comparison after scaling he pCO2 forcing to achieve best fit to the magnitude of cooling in the proxy MATs, b) Proxy-model [?]SST comparison after scaling the pCO2 forcing to achieve best fit to the magnitude of cooling in the proxy SSTs. In the Oligocene run the catchment is restricted for Prydz Bay and the Ross Sea on the basis of ice expansion reducing the effective catchment area. The grey area in the Eocene timeslice identifies the separate source regions used in Prydz Bay based on the proxy type. In the Oligocene run the catchment is restricted on the basis of ice expansion reducing the effective catchment area. In the Oligocene-Eocene panel the grey panel represents the Eocene area used for Prydz Bay while the line for source region corresponds to proxy sourcing areas for the Oligocene.

Proxy-Model Comparison for the Eocene-Oligocene Transition in Southern High Latitudes

Emily J. Tibbett[1*], Natalie J. Burls[2], David K. Hutchinson[3], Sarah J. Feakins[1]

[1]Department of Earth Science, University of Southern California, Los Angeles, CA, USA

[2]Atmospheric, Oceanic, and Earth Sciences Department, George Mason University, Fairfax, VA, USA

[3]Climate Change Research Centre, University of New South Wales, Sydney, Australia

*Corresponding author: E. J. Tibbett (tibbett@usc.edu)

Key points

- Air temperatures at the margins of the Antarctic continent dropped by 0 to 4°C across the Eocene Oligocene Transition.
- Southern high latitude sea surface temperatures cooled by 0 to 3°C.
- Best fit to the proxy surface air temperatures from CO_2-only runs suggest a 30% decrease in $p$$CO_2$ across the Eocene-Oligocene Transition.

Abstract

The Eocene-Oligocene Transition (EOT) marks the shift from greenhouse to icehouse conditions at 34 Ma, when a permanent ice sheet developed on Antarctica. Climate modeling studies have recently assessed the drivers of the transition globally. Here we revisit those experiments for a detailed study of the southern high latitudes in comparison to the growing number of mean annual sea surface temperature (SST) and mean air temperature (MAT) proxy reconstructions, allowing us to assess proxy-model temperature agreement and refine estimates for the magnitude of the $p$$CO_2$ forcing of the EOT. We compile and update published proxy temperature records on and around Antarctica for the late Eocene (38-34 Ma) and early Oligocene (34-30 Ma). Compiled SST proxies cool by up to 3°C and MAT by up to 4° between the timeslices. Proxy data were compared to previous climate model simulations representing pre- and post-EOT, typically forced with a halving of $p$$CO_2$. We scaled the model outputs to identify the magnitude of $p$$CO_2$ change needed to drive a commensurate change in temperature to best fit the

temperature proxies. The multi-model ensemble needs a 30 or 33% decrease in pCO_2, to best fit MAT or SST proxies respectively, a difference of just 3%. These proxy-model intercomparisons identify pCO_2 as the primary forcing of EOT cooling, with a magnitude (-200 or -243 ppmv) approaching that of the pCO_2 proxies (-150 ppmv). However individual model estimates span -66 to -375 ppmv, thus proxy-model uncertainties are dominated by model divergence.

Plain Language Summary

Antarctica was once a continent with little to no ice on it. Around 34 million years ago Antarctica developed its first permanent ice sheet as temperatures cooled. To evaluate how much cooling occurred on and around Antarctica, we compiled evidence from the molecules left behind by ancient organisms, that carry information about temperature, as reported previously in the literature. We then compared the ancient evidence to climate model experiments which allows us to test cause and effect. Cooling is thought to be caused by a drop in carbon dioxide concentrations in the atmosphere, and we tested how much carbon dioxide levels would need to drop to explain the cooling found. Our estimates are similar to independent evidence from marine organisms for carbon dioxide concentrations.

Keywords: EOT, DeepMIP, IODP, BAYSPLINE, BAYSPAR, BAYMBT

1. Introduction

The Eocene-Oligocene Transition (EOT) spans 34.4 to 33.7 Ma (Coxall & Pearson, 2007; Hutchinson et al., 2021; Katz et al., 2008) and marks the growth of permanent ice sheets on Antarctica (McKay et al., 2022). This transition includes a two-step increase in benthic foraminiferal $\delta^{18}O$ by 1.2‰ (Westerhold et al., 2020). The first step increase in $\delta^{18}O_{benthic}$ is harder to identify and does not appear in all records relative to the second step, referred to as the Earliest Oligocene Isotope Step (Hutchinson et al., 2021), which is an increases in $\delta^{18}O_{benthic}$ of 0.7‰ or more denoting the expansion of the Antarctic ice sheet. Estimates for the size of the ice sheet based on the benthic $\delta^{18}O$ signal suggest an ice sheet 60-130% of the modern East Antarctic Ice Sheet (Bohaty et al., 2012b; Lear et al., 2008). This transition is marked by a decrease in pCO_2 (Rae et al., 2021), temperature (Coxall & Pearson, 2007; Hutchinson et al., 2021; Lear et al., 2008; Liu et al., 2009), and sea level (Houben et al., 2012; Miller et al., 2020). An early hypothesis for the growth of permanent ice sheets on Antarctica was that gateway openings at the Drake Passage and Tasman Gateway led to thermal isolation of Antarctica (Kennett, 1977). Several ocean-only or intermediate complexity climate models suggest that the opening or deepening of the Southern Ocean gateways could have a local cooling effect close to the Antarctic coast (Sauermilch et al., 2021; Sijp et al., 2009). However, the accumulating proxy records and coupled climate modelling experiments have indicated that the gateway hypothesis does not fully explain the global cooling experienced at the EOT (e.g., Hutchinson et al., 2021; Lauretano et al., 2021). Ocean circulation proxy reconstructions indicate that the timing does not match the proposed mechanism. Deep water currents through the Tasman Gateway were first established around 30 Ma (Scher et al., 2015), i.e., after the EOT. For the Drake Passage, full opening may have occurred even later, in the Miocene (Dalziel et al., 2013).

A growing consensus is that a decrease in pCO_2 across the EOT is the primary driver for the EOT and temperature decrease globally (DeConto & Pollard, 2003; Goldner et al., 2014; Hutchinson et al., 2021; Lauretano et al., 2021; Pagani et al., 2011). Previous model proxy comparisons indicating a decrease in pCO_2 by 40% can explain the global temperature shift (Hutchinson et al., 2021). Recent pCO_2 compilations (Rae et al., 2021) constrain a decrease in pCO_2 from 980 to 830 ppmv, a 16% decrease, based on the boron isotope proxy (Anagnostou et al., 2016, 2020; Henehan et al., 2020; Pearson et al., 2009) and from 660 to 520 ppmv from alkenones, a 27% decrease, across the EOT (Pagani et al., 2005, 2011). Both proxies converge on the magnitude of the decrease being just 140-150 ppmv between the late Eocene and the early Oligocene, and when averaging across both proxies there is roughly a 25% decrease across the EOT (Rae et al., 2021). Although carbon dioxide has been established as the leading cause, additional feedbacks are invoked from both the ice-albedo feedback and gateway-induced changes to deep-water formation (Goldner et al., 2014). Several coupled climate model studies have found a shift from South Atlantic to South Pacific deep-water formation across the EOT due to Southern Ocean gateway opening (Kennedy et al., 2015; Toumoulin et al., 2020). Furthermore, deep water circulation proxies suggest that there was an expansion of North Atlantic Deep Water formation around the EOT (Coxall et al., 2018), supported by paleogeographic and modelling evidence of the Arctic becoming isolated from the North Atlantic (Hutchinson et al., 2019; Vahlenkamp et al., 2018). These studies suggest that ocean gateway and ice sheet changes could be involved in driving the observed changes at the EOT, although declining pCO_2 is the only mechanism proven to cause global cooling.

Climate models allow the drivers of change to be tested. Inter-model differences in boundary conditions (e.g., continental configuration) and parameterization schemes can lead to different outcomes. Multi-model comparisons can test the robustness of hypotheses for the transition to these differences in model formulation. One surprising feature of climate model experiments, is the finding of a smaller decrease in surface air temperatures at higher latitudes in comparison to mid-latitudes across the EOT (Kennedy-Asser et al., 2020). Model experiments also indicate Southern Ocean sea surface temperatures (SSTs) cooled more than the land at the same latitude. SST proxies indicate a global average cooling of 2.5°C across the EOT and regional differences in cooling ranging from 0 to 8°C (Hutchinson et al., 2021). Compiled global land surface mean air temperature (MAT) proxy records suggest a global mean cooling of 2.3°C with latitudinal and regional differences in cooling from 0 to 8°C (Hutchinson et al., 2021). However, proxy records are concentrated in northern mid-latitudes with limited records from the Southern Hemisphere and few from Antarctica. The sparse coverage of proxy records in the Southern Hemisphere and from Antarctica has hampered past efforts to evaluate model outputs.

We now have more temperature records to assess the magnitude of the land and sea temperature shift across the EOT surrounding the Southern Ocean. For example, there are now *br*GDGT-based temperature estimates on both sides of the Southern Ocean from Prydz Bay (Tibbett et al., 2021a) and South Australia (Lauretano et al., 2021). We add these new records to compiled proxies and multi-model experiments for the EOT (compiled by Hutchinson et al., 2021). Hutchinson et al., (2021) compiled proxy data globally, whereas we take a more in-depth look at the southern high latitudes (>45ºS) including Antarctica. For this proxy-model comparison, we update the proxy compilation using the latest calibrations and we update proxies onto a comparable timescale. In contrast to the recent high latitude study by Lauretano et al., (2021) that compared to a single climate model, we compare to the full suite of model experiments as in Hutchinson et al., (2021). While the individual model experiments generally used a halving of carbon dioxide to force a large EOT response, we scale the model experiments to identify the pCO_2 forcing required to better reproduce the temperature anomaly across the transition observed in the proxy data in the high southern latitudes. The focused multi-proxy, multi-model high latitude comparison allows us to identify sub-regional differences in the proxies and in the climate model experiments to reach new understanding of the forcing and response during the Eocene-Oligocene Transition on and around Antarctica.

2. Methods

2.1. Proxy data

Proxy temperature records were collected south of 45°S (Figure 1a) based on paleolatitudes for the late Eocene (38 to 34 Ma) and early Oligocene (34 to 30 Ma) collating records from land and sea for MAT and SST (**Figure 1b,c**). Paleocoordinates were reconstructed using the modern day drilling coordinates and (Müller et al., 2018) to reconstruct paleolatitude and paleolongitudes at 34 Ma. Proxy methods for the temperature reconstructions are noted and where appropriate the data were recalibrated to the latest methods for compatibility within the compilation (as described in the following sections on MAT and SST). Age models were updated to the GTS2012 age model (Gradstein et al., 2012) for comparability in the 4 Ma windows bracketing the EOT transition. Each of these updates (location, proxy calibration and age model can be found in the proxy synthesis (Tibbett et al., 2022a).

2.1.1. MAT

For the southern continents, reconstructions of mean annual air temperatures (MAT, **Table 1**) come from palynological analysis (Francis et al., 2008; Hunt & Poole, 2003; Macphail & Truswell, 2004; Poole et al., 2005; Truswell & Macphail, 2009), which identifies pollen grains to plant genus or species level and constrains the climate based on known temperature and precipitation ranges of the extant species or nearest living relative (NLR) (Amoo et al., 2022; Thompson et al., 2022), as a probability density function (and central estimate) of likely climatic range (Harbert & Nixon, 2015; Hollis et al., 2019; Willard et al., 2019). The temperature compilation for the continents also includes mineral weathering via the S-index climofunction (Passchier et al., 2013, 2017) which is based on the molar ratio of Na_2O and K_2O to Al_2O released during weathering (Sheldon et al., 2002).

We also compiled records using the soil bacterial biomarkers, the branched Glycerol Dialkyl Glycerol Tetraethers (*br*GDGTs). The original MBT/CBT (Cyclization of Branched Tetraethers) index (Douglas et al., 2014) includes temperature responsive methylation, but also the cyclization of *br*GDGTs, which varies with pH complicating that paleothermometer (Weijers et al., 2007). A newer method determines the MBT'_{5Me} index based only on the methylation of *br*GDGTs, which responds to temperature (Hopmans et al., 2016), an approach available after improvement in the separation of the 5- and 6-methyl *br*GDGTs (De Jonge et al., 2014; Hopmans et al., 2016). The MBT'_{5Me} index has been calibrated to temperature (both mean annual and months above freezing) with the Bayesian regression model of the Methylation of Branched Tetraethers index (BayMBT) (Dearing Crampton-Flood et al., 2020). For both the Eocene and the Oligocene cases the MAF and MAT estimates are indistinguishable. BayMBT calibrated data are reported with the calibration to mean annual air temperature for the purposes of consistency with other mean annual air temperature (MAT) proxies and the reporting conventions for proxy-model comparison. However we will return to the seasonal question and the latest calibrations to months above freezing (MAF), based on the understanding that soil microbial communities are unlikely to be active below freezing (Deng et al., 2016; Weijers et al., 2007, 2011), at the end of the discussion. All BayMBT records, from marine drill cores, were screened for additional indices (e.g., BIT and $\#Rings_{tetra}$) that can denote confounding factors similar to tests in Tibbett et al., (2022b), as no aquatic overprinting was identified for the records, none were excluded. The WW7 record is from a peat deposit and therefore is not at risk for aquatic overprinting. The MBT/CBT record cannot be recalibrated using BayMBT due to the lack of separation of the 5 and 6 methyl isomers but is retained. We have one instance of a peat-based temperature estimate (Lauretano et al., 2021) reported using the MBT_{peat} calibration (Naafs et al., 2017) that was recalibrated using BayMBT (Dearing Crampton-Flood et al., 2020), with no significant change in estimated MAT.

Table 1. Mean annual air temperature proxy compilation for late Eocene (38-34 Ma) and early Oligocene (34-30 Ma).
* Douglas et al., (2014) also reported MBT′/CBT, excluded as unrealistically warm. **Pollen-based

				Late Eocene MAT		Early Oligocene MAT		O-E	
Location	Lat	Long	Proxy	Mean (ºC)	1σ (ºC)	Mean (ºC)	1σ (ºC)	Δ(ºC)	Reference
739, 742,1166	-67.3	75.1	BayMBT	11.0	2.0	6.8	2.6	-4.2	Tibbett et al., 2021b
739, 742,1166	-67.3	75.1	S-index	10.4	1.0	8.1	0.5	-2.3	Passchier et al., 2017
CIROS-1 CRP Sites 2/3	-77.7	163.5	S-index	8.7	1.2	7.8	1.3	-0.9	Passchier et al., 2013
U1356	-63.3	136.0	S-index			8.9	1.2		Passchier et al., 2013
WW7	-38.2	147.1	BayMBT	23.3	1.6	20.2	1.2	-3.1	Lauretano et al., 2021 recalibrated using BayMBT
Seymour Island	-64.4	-56.8	MBT/CBT*	12.2	2.3				Douglas et al., 2014
King George Island, Dragon Glacier	-62.1	-58.9	Pollen**	12.0					Hunt & Poole, 2003; Poole et al., 2005
King George Island, Fossil Hill	-62.1	-58.9	Pollen**	13.3					Poole et al., 2005
McMurdo	-77.6	166.4	Pollen**	13.0					Francis et al., 2008
King George Island, South Sheltand Island	-62.0	-58.4	Pollen**	13.4					Francis et al., 2008
1166	-67.3	75.1	Pollen**	12.0					Macphail & Truswell, 2004; Truswell & Macphail, 2009
CRP-3	-77.0	163.7	Pollen**			6.5			Francis et al., 2008
SHALDRIL	-63.8	-54.7	BayMBT	6.9	0.5				Tibbett et al., 2022c
696	-61.8	-42.9	Pollen	11.9	1.8	11.2	1.0	-0.7	Thompson et al., 2022
1172	-43.9	158.3	Pollen	11.7	1.7	11.9	1.7	+0.2	Amoo et al., 2022

temperature estimates are reported here as MAT. Standard deviations represent timeseries variability. Latitude and longitude are reported for present positions and are reported to 0.1° resolution.

2.1.2. SST

Southern high latitude SST records (**Table 2**) are from the archaeal membrane lipid TEX_{86} index (Douglas et al., 2014; Hartman et al., 2018; Lauretano et al., 2021; Tibbett et al., 2021a) which is based on the relationship between SST and the degree of cyclization of isoprenoidal GDGTs (isoGDGTs) produced by Crenarchaeota (Schouten et al., 2002). Additional SST records include the haptophyte algal biomarker $U^{k'}_{37}$ index (Houben et al., 2019; Liu et al., 2009; Pagani et al., 2011; Plancq et al., 2014) produced by Reticulofenestrids in the Eocene and Oligocene (Henderiks & Pagani, 2008). The $U^{k'}_{37}$ index SST relationship is based on the proportion of di- and tri-unsaturated C_{37} alkenones (Prahl & Wakeham, 1987; Sikes et al., 1997; Sikes & Volkman, 1993). Carbonate clumped isotopes Δ_{47} values measured on shallow coastal bivalves were also included as SST proxies (Douglas et al., 2014; Petersen & Schrag, 2015) since "clumped" ^{18}O-^{13}C is responsive to temperature (Ghosh et al., 2006). For Douglas et al., 2014 the TEX_{86} SSTs were reevaluated using BAYSPAR (Bayesian, Spatially-Varying Regression calibration for TEX_{86}) (Tierney & Tingley, 2014) with a prior of 13°C and a standard deviation of 15°C. Other TEX_{86} records from the Southern Ocean were either originally calibrated with BAYSPAR (Hartman et al., 2018; Lauretano et al., 2021; Tibbett et al., 2021a), or were recently reevaluated using BAYSPAR (Lauretano et al., 2021) with priors ranging from 12 to 21°C and a standard deviation of 20°C. The $U^{k'}_{37}$ records were reinterpreted using the latest BAYSPLINE (B-spline fit with a Bayesian regression) calibration (Tierney & Tingley, 2018).

Table 2. Sea surface temperature proxy compilation for the late Eocene (38-34 Ma) and early Oligocene (34-30 Ma)

				l. Eocene SST		e. Oligocene SST		O-E	
Site	Lat	Long	Proxy	Mean (ºC)	1σ (ºC)	Mean (ºC)	1σ (ºC)	Δ (ºC)	Reference
739, 742, 1166	-67.3	75.1	BAYSPAR	12.6	1.7	10.4	1.1	-2.2	Tibbett et al., 2021b
689	-64.5	-3.1	Δ_{47}	13.3	5.0	12.0	0.9	-1.3	Petersen & Schrag, 2015
511	-51.0	-47.0	BAYSPAR	15.7	2.1	13.1	1.0	-2.6	Houben et al., 2019 * Lauretano et al., 2021
511	-51.0	-47.0	BAYSPLINE	17.6	2.1	10.8[x]	2.5	-6.8	Houben et al., 2019[#],**

511	-51.0	-47.0	BAYSPLINE	18.2	2.5	10.7[x]	0.8	-7.5	Liu et al., 2009; Plancq et al., 2014, from Elsworth et al., 2017 **
277	-52.2	166.2	BAYSPAR	26.6	1.1	24.0	0.4	-2.6	Pagani et al., 2011,* Lauretano et al., 2021
277	-52.2	166.2	BAYSPLINE	25.4	1.8	23.1	2.0	-2.3	Pagani et al., 2011 **
1172	-43.9	158.3	BAYSPAR	20.5	1.1	20.5	0.9	0	Houben et al., 2019 * from Lauretano et al., 2021
U1356	-63.3	136.0	BAYSPAR			18.7	2.0		Hartman et al., 2018
Seymour Island	-64.4	-56.8	BAYSPAR	13.5	2.1				Douglas et al., 2014 *
Seymour Island	-64.4	-56.8	Δ_{47}	12.9	0.7				Douglas et al., 2014

*TEX_{86} recalibrated from original publication with BAYSPAR. ** $U^{k'}_{37}$ recalibrated with BAYSPLINE. Standard deviations represent timeseries variability. Latitude and longitude are reported for present positions and are reported to 0.1° resolution. # DSDP Site 511 SST reconstruction (Houben et al., 2019) updated with ages from Lauretano et al., (2021). [x]Site 511 has two BAYSPLINE entries, both with anomalous Oligocene cooling, that are excluded from the proxy-model comparison.

2.1.3. Proxy Uncertainty

Proxy uncertainty varies by proxy and is defined in the original calibration studies for each proxy, although the uncertainty is necessarily less well known in application to the past. For the GDGT-based proxies, SST and MAT values estimated by BAYSPAR and BayMBT respectively, carry one standard deviation calibration uncertainty ca. 4°C. The standard error reported for the linear regression of MBT/CBT to temperature is 5.5°C (Weijers et al., 2011). The $U^{k'}_{37}$ BAYSPLINE calibration carries a standard deviation of ca. 4°C (Tierney & Tingley, 2018). For clumped isotopes uncertainties come from instrument error, sample heterogeneity and accuracy summarized as 2.5°C in the Seymour Island study (Douglas et al., 2014). Pollen temperatures generated from nearest living relative analysis are reported to have a standard deviation of 2 to 3°C (Amoo et al., 2022; Thompson et al., 2022). For S-index the reported calibration standard deviation is 3.6°C (Sheldon et al., 2002). The approaches used to quantify uncertainty do vary between calibration approaches, with the error propagation captured rigorously in the bayesian calibrations and may be underreported in other cases. Beyond calibration uncertainty, the uncertainty around the central estimate for each timeslice is dependent upon the number of data points and the variability and length of the window chosen. For the intervals chosen here we report the standard deviation for each timeseries representing the variability around the means for each timeslice (**Table 1**

and 2). The selection of a longer time window can lead to more time averaging and thus dampening of the magnitude of the transition, as will be explored in the results.

At sites with multi-proxy reconstructions, we can assess the direction and magnitude of proxy-proxy discrepancy at each site and for each timeslice, and we can test sensitivity to the exclusion of single reconstructions and proxy types in addition to the comparison of MAT versus SST proxies which are also independent assemblages of data. As an example for land proxies, archived in marine sediments at Prydz Bay the difference between the S-index and BayMBT is up to 4°C. The S-index is cooler due to inferred higher elevation sourcing of the rock-erosion proxy (S-index) versus the lower elevation (warmer) sourcing of soil microbial biomarkers (Tibbett et al., 2021a). For the SST proxies, at Site 277 both BAYSPAR and BAYSPLINE agree within error with cooling of 2.2 and 2.6°C respectively across the EOT (Lauretano et al., 2021; Pagani et al., 2011). These two proxies agree despite different producers: haptophyte algae which produce alkenones (for the $U^{k'}_{37}$ index and BAYSPLINE) are primary producers and are found in the photic zone (Popp et al., 2006; Volkman et al., 1980), whereas Thaumarchaeota (producers of *iso*GDGTs used for TEX_{86} and BAYSPAR) were more abundant in the subsurface of the Southern Ocean (Kalanetra et al., 2009), raising the possibility that proxy-proxy discrepancies may in part arise from different depth habitats when there is a vertical gradient in ocean temperatures. Offsets may also relate to lateral advection of alkenones, and one place where this has previously been anomalous has been is on the Brazilian margin (Tierney and Tingley, 2018). In the same margin, at DSDP Site 511 alkenones record an anomalous cooling of ~8°C (Houben et al., 2019) interpreted with BAYSPLINE, whereas at the same site the TEX_{86} proxy interpreted with BAYSPAR records ~3°C cooling (Lauretano et al., 2021) consistent with other high southern latitude EOT reconstructions. We exclude the anomalous cooling inferred from alkenones (BAYSPLINE) at Site 511 (**Table 2**) from proxy-model comparison, but we do perform a sensitivity test to show the worst case scenario proxy-proxy disagreement.

2.2. Models

We re-use the ensemble of model experiments gathered onto a uniform grid used in the HadCM3BL model by Hutchinson et al., (2021). The initial grid resolution can be found in the original papers (**Table 3**) for each model simulation (Baatsen et al., 2020; Goldner et al., 2014; Hutchinson et al., 2018, 2019; Ladant, et al., 2014a; Ladant et al., 2014b; Sijp et al., 2016; Zhang et al., 2014; Zhang et al., 2012) The compiled experiments include two broad groupings 4x CO_2 (Eocene-like high pCO_2) and 2x CO_2 (Oligocene-like low CO_2) each run without ice sheets to isolate only the effects of changing pCO_2 (**Table 3**). Additional model runs were included for a subset of models to compare other EOT drivers which included the paleogeography changes across the EOT (CESM_H, GFDL CM2.1, HadCM3BL, FOAM, UViC, NorESM-L), and the inclusion of an ice sheet (CESM_H, FOAM, HadCM3BL) (**Table 3**). In addition, an ensemble mean for each comparison was obtained by averaging across the model simulations. The pCO_2 (2x vs 4x), paleogeography (pre-EOT vs post-EOT), and ice (no ice vs ice sheet) compared parameters can be found in Table 3. More detailed information on the boundary conditions for each simulation used can be found in the supplement (**Text S1**). In addition, all models used in each comparison were averaged to generate an ensemble mean for each analysis performed. A correction was applied to the NorESM-L model simulation that originally used a pCO_2 drop from 980 to 560 ppmv. This was scaled by Hutchinson et al., (2021) to match the 4x/2x simulations (50% reduction in pCO_2 across the EOT) in the other models and maintained here. The summary of the model parameters can be found in **Table 3** and detailed model run information for each of the models in the ensemble can be found in Hutchinson et al., (2021; and references therein). Here, we scale the model outputs to the proxy temperature differences to identify the pCO_2 decrease across the EOT. As in the approach of Hutchinson et al., (2021), the 2x-4x pCO_2 (Oligocene-Eocene) model results were scaled by a constant, ranging from 0 to 2, with 1 representing a 50% decrease (2x-4x pCO_2), from the initial models, to determine the forcing required to achieve the best fit between the proxies and the model for each simulation. Although commonly referred to as surface air temperature (SAT) in the model literature, we refer to land surface mean air temperatures as MAT, to be consistent with the proxy literature.

Table 3. Model simulation parameters compared for each set of paired model runs

Model	pCO_2 (ppmv) model simulations		ice model simulations (volume km^3)		paleogeography model simulations		Reference
	Eocene	Olig.	Eocene	Olig.	Eocene	Olig.	
CESM_B	1120	560	no ice		38 Ma (no paleogeography changes between timeslices)		Baatsen et al., 2020
CESM_H	1120	560	no ice	$20.3x10^6$	Drake and Tasman closed	Drake and Tasman open	Goldner et al., 2014
FOAM	1120	560	no ice	$25.0x10^6$	WA below sea level	WA above sea level	Ladant et al., 2014a; Ladant., et al., 2014b
GFDL CM2.1	800	400	no ice		Arctic gateway open	Arctic gateway closed	Hutchinson et al., 2018, 2019
HadCM3BL	1120	560	no ice	$17.0x10^6$	Priabonian reconstruction	Chattian reconstruction	Kennedy et al., 2015
NorESM-L	1120 (980 initial)	560	no ice		35 Ma reconstruction	33 Ma reconstruction	Zhang et al., 2012, 2014
UViC	1600	1600	no ice		Drake closed	Drake Open	Sijp et al., 2016

Three sets of model simulations were compared pCO_2 high vs low (4x vs 2x), no ice vs ice simulations, and paleogeographic simulations pre-EOT and post-EOT. The simulations outside of the pairings do not have the same conditions (**Text S1**). For models with more than one parameter all other factors held constant. NorESM-L was scaled to 1120 ppmv. For the ice/no ice runs pCO_2 is held constant at 560 ppmv. For the paleogeography runs the pCO_2 for both pre- and post-EOT is 1120 ppmv for CESM_H, 560 ppmv for FOAM, HadCM3BL and NorESM-L, 800 ppmv for GFDL CM2.1, and 1600 ppmv for UViC. Drake = Drake Passage, Tasman = Tasman Gateway, WA = West Antarctica, Olig = Oligocene.

Where land temperature proxies (e.g., soil bacterial biomarkers or soil weathering indicators) were recovered from marine sedimentary archives, we inferred sourcing from the adjacent continent. Source regions were defined on the adjacent land mass, averaging the modelled surface temperatures within an area reflective of Antarctic drainage basins. The source region was adjusted for the Prydz Bay BayMBT record as the organic material is likely sourced from the lowland soils (Tibbett et al., 2021a) with sourcing based on topography reconstruction at 34 Ma (Paxman et al., 2019). The Oligocene source region was adjusted for land proxy records from Pyrdz Bay and from the Ross Sea as ice growth means they were likely limited to coastal sourcing (Van Breedam et al., 2022), while records from Wilkes Land were not limited to the coast as the East Antarctic Ice Sheet was determined to be further inland (Paxman et al., 2018).

For SST proxies we assume they capture temperatures in the overlying water column at the marine core site and thus compare to the nearest grid point within the model. In cases where marine archives appeared to plot "on land" due to modelled coastline imprecision, we obtained model comparison points from the nearest ocean grid cell for comparison to the marine core derived SST proxies. The proxy-model intercomparison differences are expressed as root mean square error (RMSE) (equation 1) with n as the number of proxies. This was assessed for each model scenario (Eocene and Oligocene) and the difference between the two.

$$RMSE = \sqrt{\frac{\sum_{i=1}^{n}(model - proxy)^2}{n}} \quad (1)$$

2.2.1 Sensitivity to proxy spatial coverage and model heterogeneity

To evaluate how the availability of additional proxy data might potentially improve comparisons with climate models, we performed a model sensitivity test, to an increasing number of constraints, while also illuminating the existing model limitations through model-model comparisons. First, we assigned one "perfect" model simulation as having the "true" temperature and using the same proxy sampling site locations as used in our initial proxy-model comparison we compared to each of the other models to evaluate the error. We then modeled the effect of adding all possible marine grid cells from 45°S to the Antarctic coastline for SST (n=710) and all possible land grid cells (n=960) from 60°S to 90°S for MAT comparisons. This type of approach helps to constrain uncertainties that derive from inter-model differences, which are hidden by the model ensemble approach.

3. Results

3.1. Temperature change in the proxies

The compiled temperature proxies' distributions (**Figure 1a**), and timeseries are presented for MAT (**Figure 1b**) and SST (**Figure 1c**). Although the EOT cooling is hidden by the spread of temperatures across latitudes (**Figure 1b,c**) after parsing the data by region and calculating the cooling anomalies relative to the Eocene, the EOT cooling pattern emerges more clearly (**Figure 1d, e**) as a significant shift in regional climate, that is linked to the global features of forcing and ice volume and deep ocean temperature represented by $\delta^{18}O_{benthic}$ (**Figure 1f**). While the details of each timeseries have been explored in the original publications, here we summarize the data for individual proxy and sites, for MAT (**Table 1**) and SST proxies (**Table 2**) for the 4 Ma windows bracketing the EOT. We use the mean values for the late Eocene (38-34 Ma) and early Oligocene (34-30 Ma) for the proxy-model comparisons, and, thus we are able to make use of records that only constrain one or either time period as well as those that span the transition.

3.1.1. Time-averaging of variable timeseries

Averaging may attenuate the magnitude of EOT cooling, for example where a rebound in temperature occurs post-EOT (Bohaty et al., 2012a; Tibbett et al., 2021b) perhaps linked to a rebound in pCO_2 (Pearson et al., 2009, Anagnostou et al., 2020). At Prydz Bay, cooling at the EOT was reported to be 5°C and 4°C for MAT and SST respectively (Tibbett et al., 2021a), but by averaging across the bracketing 4 Ma windows (38-34 and 34-30 Ma), the early Oligocene to late Eocene cooling is 4.2°C and 2.2°C for SST and MAT respectively – i.e., averaging dampens the calculated cooling by 30-45%. To assess sensitivity of the pCO_2 scaling to the selected window length we compared the effects of averaging 4, 2 and 1 Ma pre and post-EOT. The MAT RMSE for 4 Ma averages ranged from 1.38 to 2.34°C with a pCO_2 decrease of 11 to 30%. Using a 2 Ma window the RMSE ranged from 1.38 to 2.44°C with a pCO_2 decrease of 6 to 29% and for 1 Ma the RMSE ranged from 1.58 to 2.55°C with a pCO_2 decrease of 17 to 40%. The SST RMSE for 4 Ma averages ranged from 0.90 to 1.45°C with a pCO_2 decrease of 21 to 46%. Using a 2 Ma window the RMSE ranged from 0.52 to 0.80°C with a pCO_2 decrease of 18 to 44% and for 1 Ma the RMSE ranged from 1.28 to 2.19°C with a pCO_2 decrease of 32 to 70% (**Supplemental Table S6 and S7)**. As we saw no significant improvement for both MAT and SST with other windows, we maintain the 4 Ma windows to best capture proxy availability.

3.2. Temperature change in the model simulations

3.2.1. pCO_2 model simulations

To compare the model simulations for the Antarctic the MAT was limited to >60°S and for SST >45°S. The Antarctic temperature change between the Oligocene and Eocene model simulations reflects a 50% decrease in pCO_2. For the MAT model simulations the CESM_B (O-E) temperature difference ranges from -6.4 to -2.3°C with a mean of -4.0°C, for CESM_H it ranges from -6.3 to -1.9°C with a mean of -3.9°C, GFDL CM2.1 ranges from -9.8 to -3.9°C with a mean of -6.6°C, HadCM3BL ranges from -15.0 to +4.5°C with a mean of -2.4°C, FOAM ranges from -6.5 to -2.7°C with a mean of -4.3°C, NorESM-L ranges from -6.7 to 0.0°C with a mean of -3.3°C, and the ensemble mean of the 6 models (excluding UviC as there were no simulations for a change in pCO_2) ranges from -7.3 to -2.1°C with a mean of -4.1°C. The models exhibit an average decrease of -4.1°C for MAT from the Eocene to the Oligocene for the 50% decrease in pCO_2 simulated for the Antarctic. For SST the CESM_B Antarctic temperature change between the Oligocene and Eocene timeslice ranges from -4.4 to -1.8°C with a mean of -3.1°C, for CESM_H it ranges from -4.8 to -1.9°C with a mean of -3.3°C, GFDL CM2.1 ranges from -9.6 to -3.8°C with a mean of -5.2°C, HadCM3BL ranges from -4.3 to +4.4°C with a mean of -1.2°C, FOAM ranges from -7.5 to -1.9°C with a mean of -3.7°C, NorESM-L ranges from -3.7 to +0.4°C with a mean of –1.6°C, and the ensemble mean of the 6 models, excluding UviC, ranging from -9.5 to -0.5°C with a mean of -3.2°C. For the SST 50% decrease in pCO_2 model simulations, the average decrease in temperature for the Antarctic from the Eocene to Oligocene is -3.0°C.

3.2.2. Ice sheet model simulations

Following the same geographic constraints as above we report the model temperature difference between the no ice (Eocene) and ice sheet (Oligocene). For CESM_H the temperature ranges from -41.1 to +1.1°C with a mean of -12.0°C, HadCM3BL ranges from -37.2 to +6.6°C with a mean of -11.2°C, FOAM ranges from -37.4 to +3.2°C with a mean of -14.7°C, and the ensemble mean ranges from -37.6 to +0.5°C with a mean of -13.3°C. For SST, CESM_H ranges from -8.8 to +1.6°C with a mean of -1.2°C, HadCM3BL ranges from -2.4 to +3.3°C with a mean of -0.3°C, FOAM ranges from -6.0 to +2.7°C with a mean of +0.1°C, and the ensemble mean ranges from -8.8 to +1.5°C with a mean of -0.8°C. The average change in temperature across the 3 model simulations, excluding the ensemble mean, is -12.6°C and -0.5°C for MAT and SST respectively.

3.2.3. Paleogeography model simulations

The model simulation temperature difference between the pre-EOT and post-EOT paleogeographies vary by model. For MAT CESM_H ranges from -1.9 to +3.7°C with a mean of +0.1°C, GFDL_CM2.1 ranges from +0.6 to +2.2°C with a mean of +1.4°C, HadCM3BL ranges from -9.6 to +19.1°C with a mean of +1.9°C, FOAM ranges from -5.0 to +2.2°C with a mean of -0.3°C, UviC ranges from -2.0 to +1.3°C with a mean of -0.8°C, NorESM-L ranges from -2.4 to +1.4°C with a mean of -0.1°C, and the ensemble mean it ranges from -2.6 to +3.4°C with a mean of +0.4°C. For SST CESM_H ranges from -2.0 to +1.5°C with a mean of -0.3°C, GFDL_CM2.1 ranges from -0.6 to +3.0°C with a mean of 1.2°C, HadCM3BL ranges from -2.3 to +4.5°C with a mean of +1.5°C, FOAM ranges from -4.4 to +1.8°C with a mean of -1.2°C, UviC ranges from -4.2 to +7.0°C with a mean of -0.5°C, NorESM-L ranges from -3.2 to 1.9°C with a mean of -0.4°C, and the ensemble mean ranges from -3.5 to +2.6°C with a mean of +0.1°C. The average change across the EOT, excluding the ensemble mean, comparing the paleogeography runs is +0.1 for SST°C and +0.4°C for MAT.

3.3. Proxy-model temperature comparison

3.3.1. Temperature comparison within "pCO$_2$ runs" without an ice sheet

For the pCO$_2$ runs, the RMSE for the MAT ranges from 4.6 to 7.9°C for the Eocene, 5.0 to 7.3°C for the Oligocene, and 2.3 to 3.6°C for the difference comparison (**Figure 2 and Figure S1**). The RMSE for the SST ranges from 4.6 to 8.7°C for the Eocene, 5.2 to 9.4°C for the Oligocene, and 1.2 to 3.5°C for the temperature comparison (**Figure 3 and Figure S3**). The best fit for the Eocene data is CESM_B for both MAT and SSTs (4.6°C); however, for MAT CESM_H and GFDL CM2.1 also had an RMSE of 4.6°C as well as GFDL CM2.1 for SST. All three models for MAT had the same RMSE for the Oligocene timslice which was the lowest RMSE (5.7°C) and CESM_B had the lowest for SSTs (5.2°C). The lowest RMSE for the 2x-4x pCO$_2$ comparison comes from FOAM of 2.4°C for MAT and for SSTs the lowest RMSE was 1.2°C from HadCM3BL. Although they have the best fit to the data this would imply a higher pCO_2 decrease given the difference between the Eocene and Oligocene runs is a halving of pCO_2. The ensemble mean RMSE, for a halving of pCO_2, is 2.3°C and 1.6°C for MATs and SSTs respectively.

3.3.2. Temperature comparison with the "ice sheet" runs

For the ice sheet comparison only 3 models were used (CESM_H, HadCM3BL, and FOAM) as well as the ensemble mean. The RMSE for MAT ranged from 7.9 to 10.4°C for the Eocene, 10.5 to 15.4°C for the Oligocene, and 2.7 to 8.1°C for the ice-no ice comparison (**Figure 4 and Figure S4**). The RMSE for SST ranged from 8.6 to 10.3°C for the Eocene, 7.5 to 8.8°C for the Oligocene, and 1.6 to 2.5°C for the ice-no ice comparison (**Figure 4 and Figure S5**). The lowest RMSE for both MAT and SST for the difference comparison is HadCM3BL. FOAM has the highest RMSE across all three time slices for SST. The Eocene MAT no ice runs have a higher RMSE (average of ~9°C when excluding the ensemble mean) compared to the MAT Eocene pCO_2 run RMSE (average of ~6°C excluding the ensemble mean) which are run at a higher pCO2 (800-1120 ppmv versus 560 ppmv for Eocene ice runs) indicating that a high pCO_2 is needed to better reflect Eocene temperatures. For the Oligocene there are substantial proxy-model discrepancies (high RMSE) for MAT. Proxies confidently identify MAT above freezing, whereas the climate models forced with a large difference between the ice and no ice runs yields, as high as -40°C (**Section 3.3.2**), too large a cooling compared to proxies.

3.3.3. Temperature comparison within the "Paleogeography" runs

Paleogeography was changed across all models except CESM_B, and to isolate the effects of paleogeography, pCO_2 was held constant between the Eocene and Oligocene runs. CESM_H, GDFL CM2.1, and UViC reflect changes in ocean gateways (**Table 3**). CESM_H contrasts Tasman and Drake passage closed pre-EOT and open post-EOT. GDFL CM2.1 simulations have the Arctic Gateway open pre-EOT and closed post-EOT, and UViC has the Drake Passage closed pre-EOT and open post-EOT. FOAM has West Antarctica above sea level in the Eocene and mostly below sea level in the Oligocene representation. HadCM3BL model slight changes in continental positions from the Late Eocene to early Oligocene with a small shift in latitude and longitude as well as the coastline (**Figure S6 and S7**; as well as Figure S3 in Hutchinson et al., 2021). NorESM-L also models paleogeography changes; however, these changes are found at latitudes ranging from 0 to 30°N with no change in the Antarctic continental position or coastline between the Eocene and Oligocene timeslices (**Figure S6 and S7,** as well as Figure S3 in Hutchinson et al., 2021). The RMSE for MAT ranged from 4.6 to 10.8°C for the Eocene, 2.9 to 8.8°C for the Oligocene, and 3.5 to 6.5°C for the difference (post-EOT-pre-EOT) comparison (**Figure 4 and Figure S6**). The RMSE for SST ranged from 4.6 to 10.3°C for the Eocene, 4.3 to 11.8°C for the Oligocene, and 1.9 to 4.1°C for the difference comparison (**Figure 4 and Figure S7**). The difference ensemble mean for MAT is 4.6°C and for SST is 2.3°C. The MAT for the GFDL CM2.1 run has the lowest RMSE of 4.6°C for the Eocene and CESM_H has the lowest RMSE of 2.9°C for the Oligocene. For the Eocene and Oligocene SST runs GFDL CM2.1 had the lowest RMSE of 4.6°C for the Eocene and UViC had the lowest RMSE of 4.3°C for the Oligocene. For the difference between the paleogeography for each model run the lowest RMSE was 3.5°C from UViC for MAT and 1.8°C from FOAM for SST (**Figure S6 and S7**). The best fit to the Eocene data is from the model with the lowest $p\mathrm{CO_2}$ of 800 ppmv compared to the other models with $p\mathrm{CO_2}$ of 1120 ppmv and 1600 ppmv for UViC. Most of the models suggest a warming in MAT with regional differences (**Figure S6**). This in contrast to the proxy data which suggest temperature changes of 0 to -4°C. The model with the best fit for post/pre paleogeography is FOAM which has the most cooling regionally. To note additional regional differences UViC indicates more warming in the Pacific and Ross Sea sectors of the Southern Ocean while CESM_H suggest warming in the Atlantic and Indian Ocean sector with a cooling in the Pacific and Ross Sea sectors. This difference could be attributed to the prescribed modeled gateway opening in the Southern Ocean with CESM_H modeling the opening of Drake Passage and the Tasman Gateway and UViC modeling the opening of only Drake Passage. The overall warming trend suggests that paleogeography is not the primary driver of hemispheric cooling as previously noted (Hutchinson et al., 2021; Kennedy-Asser et al., 2020) but could impact regional differences in combination with $p\mathrm{CO_2}$. It is plausible that paleogeography changes could have indirectly triggered pCO_2 changes. Two such mechanisms include a shift in the dominant basin of deep-water formation changing the ocean's ability to store carbon (Fyke et al., 2015; Speelman et al., 2009), or through land-based CO_2 weathering feedbacks triggered by the onset of the Atlantic meridional overturning circulation (Elsworth et al., 2017).

3.4. CO_2 scaling

Here we compare the updated Antarctic proxy record (rather than the global proxy data) with scaled pCO_2 to both surface air temperature and sea surface temperature. For the pCO_2 decrease calculations the assumed post-EOT pCO_2 is set at 560 ppmv, since this matches most of the models. RMSE was calculated between the difference between the 2x-4x pCO_2 runs and the Oligocene-Eocene proxies for both MAT and SST. By varying the scaling factor, we found the lowest RMSE and the best estimated decrease in pCO_2 for each model for MAT and SST proxies separately (**Figure 5**, **Table S1**). Averaging across all models (excluding the model ensemble mean), the average pCO_2 decrease is 170 ppmv for MAT and 234 ppmv for SST. This is equivalent to a 23 or 35% pCO_2 decrease when averaging all models excluding the model ensemble mean. The ensemble mean indicates a decrease of pCO_2 of 30.3 and 33.1% across the Eocene-Oligocene Transition for MAT and SST respectively, equivalent to ~200 and ~234 ppmv. The difference of 3% is a measure of the proxy derived uncertainty, between two independent ensembles of proxies, used to perform the scaling experiments.

There are however large differences between individual models. The largest decrease in pCO_2 is required in the HadCM3BL (362 ppmv) and NorESM-L (375 ppmv) climate models when fitting to the proxy SST data. When fitting to the smaller MAT difference, commensurately smaller changes are needed, with the largest changes needed in CESM_H (221 ppmv) and FOAM (232 ppmv) when matching the shift in MAT. The lowest RMSE for MAT is 1.35°C and for SST it is 1.92°C for the GFDLCM 2.1 and CESM_H model experiments respectively. Although the RMSE range is small, ranging from 1.4 to 2.3°C for MAT and 2.0 to 2.3°C for SST. SSTs have the highest range in pCO_2 percent decrease (29.3 to 60.5%) in comparison to the MATs (10.5 to 30.3%) (**Table S1**). This implies larger model discrepancy in ocean conditions than on land. Overall, a much larger proportion of uncertainty derives from model rather than proxy uncertainty.

4. Discussion

4.1. Biases in proxy temperature records

Land temperature proxies carry uncertainties in absolute temperatures. For the S-index the absolute temperatures can be cool-biased (Sheldon & Tabor, 2009), and although attempts were made to account for recycling (Passchier et al., 2013, 2017), temperatures were cold-biased compared to soil biomarkers (Tibbett et al., 2021a), in predictable ways based on differing source regions. In this study we alter the source regions in the models to better represent the varying source regions (**Figure S2**). The nearest living relative (NLR) approach assumes that the climate tolerances of past species are similar to their modern relatives (Hollis et al., 2019) and uncertainty depends on the quality of modern data and identification of fossil taxa (Utescher et al., 2014). As usual, the best way to corroborate such uncertainties is through cross checks with independent data such as that available from leaf traits (Pound & Salzmann, 2017) and temperature reconstructions included here (Lauretano et al., 2021; Tibbett et al., 2021a) that support the nearest living relative results (Amoo et al., 2022; Thompson et al., 2022).

In almost all cases SST proxy-proxy agreement is good except at DSDP Site 511, on the Falkland Plateau, in the Atlantic Ocean, where the alkenone show an anomalous cooling and were excluded. Elsewhere, the proxies broadly agree thus there is likely no consistent proxy bias in terms of depth of production, seasonality or evolutionary changes not accounted for by calibration. Lateral advection of the alkenones is a likely explanation for offsets, and we note has previously led to the exclusion of data in this region from the modern datasets for the global calibration (Tierney & Tingley, 2018). Beyond the physical reasons for the offsets in the two proxies at Site 511, that are necessarily inadequately constrained for the ancient ocean, we can evaluate the numerical implications of the proxy uncertainty. As a worst-case scenario of proxy disagreement, we test inclusion of the anomalous Site 511 alkenone data. The anomalously large cooling (~8°C) leads to a large proxy-model RMSE 2.07°C and leads to the largest calculated $p\text{CO}_2$

decrease across the EOT (44.1%), larger than proxy estimates. Our exclusion of this outlier reduces the *p*CO_2 scaling to a 33.1% decrease in *p*CO_2, in line with proxy estimates (Rae et al., 2021) and the RMSE reduces to 1.01°C, making this the preferred choice. However, we note the low number of sites available (n=6) limits the robustness of this CO_2 scaling exercise overall.

We performed the same proxy-model temperature comparison, sequentially eliminating individual records. For SST (n=5), there was no significant improvement in RMSE other than for the removal of Site 511 BAYSPLINE (**Supplemental Table S8).** The analysis was also performed by eliminating proxy types which for SST were BAYSPAR, BAYSPLINE, and clumped isotopes (**Supplemental Table S10)**. For MAT (n=5) there was no significant improvement to the RMSE by removing individual site (**Supplemental Table S9**). For MAT the proxy sets that were removed to evaluate the impact on the results were BayMBT, S-index, and pollen analysis (both NLR and pollen assemblage), with no notable effect (**Supplemental Table S11)**. However, we acknowledge the small number of proxies (n=6) for comparison.

To evaluate how the availability of additional marine core site SST and MAT reconstructions might improve comparisons with climate models, we performed a "perfect-model" sensitivity test, to an increasing number of constraints from the synthetic data first from the model grid cells corresponding to the proxy site locations and then from all available grid cells. Using only the "proxy sites" to compare between modelled SST values, the individual models converged on a 50% decrease in *p*CO_2 (**Figure S12**). For MAT, there is a larger discrepancy amongst models regarding the *p*CO_2 change, likely due to land boundary condition differences especially topography. We then modeled the effect of adding all possible marine grid cells from 45°S to the Antarctic coastline for SST (n=710) and all possible land grid cells (n=960) from 60°S to 90°S for MAT comparisons. For most of the models the RMSE increased slightly between the initial model comparison with the prescribed proxy sites and the use of all the model grid cells. The ensemble mean increased from 1.37 to 1.42°C for MAT and 1.09 to 1.18°C for SST (**Fig S5**). Based on the minimal change in the RMSE from a low number of sites (n=6 MAT, n=7 SST) to the maximum number of grid cells (n=960 MAT, n=710 SST) it does not appear that the number of proxies is the limiting factor in proxy-model comparison. Instead, the uncertainty in our proxy-model comparisons is primarily driven by discrepancies between the model simulations in terms of the climate sensitivity to the halving of CO_2. Additionally, for MAT where the specified source region changes between the Eocene and Oligocene timeslice model differences in spatial pattern of prescribed model boundary conditions becomes a source of model spread. This analysis was therefore repeated assuming a constant surface area for the Eocene and Oligocene timeslices and the model mean then better reflect a 50% decrease using this perfect model approach. This improvement highlights a tradeoff between better representing the source regions and an additional source of model uncertainty due to the differences in topography.

4.2. Ice sheet extent and ocean circulation

Ice sheet model runs suggest SST cooling in all models with regional differences, although the RMSE is higher than in the other proxy-model comparisons **(Figure S5**). Previous modeling studies found the growth of the Antarctic ice sheet had a larger effect on SSTs than changing paleogeography (Goldner et al., 2014). The model studies show how growing ice sheets served as a positive feedback on ocean circulation changes and $p\mathrm{CO}_2$ drawdown and cooling. Proxy data show the initiation of Atlantic meridional overturning circulation during the late Eocene/EOT (Coxall et al., 2018). The models used in this study have regional differences in warming and cooling around the Antarctic continent in response to the ice sheet and different feedbacks within the models, and their different boundary conditions. For example, FOAM shows warming in the Southern Ocean while CESM_H shows cooling primarily with some warming in the Indian and Pacific Ocean sectors (**Figure S5**).

The defining feature of the Eocene Oligocene Transition is the glaciation of Antarctica. The model runs used to represent the Oligocene in this comparison have prescribed ice sheet sizes ranging from $17\mathrm{x}10^6$, $20\mathrm{x}10^6$, and $25\ \mathrm{x}10^6\ \mathrm{km}^3$ for HadCM3BL, CESM_H, and FOAM respectively (Goldner et al., 2014; Kennedy et al., 2015; Ladant et al., 2014a; Ladant et al., 2014b). These ice volumes correspond to

~65%, 75% and 95% of the modern Antarctic ice sheet respectively, which fall within estimates from benthic $\delta^{18}O$ that place the EAIS at 60-130% of the modern EAIS, with uncertainty due to the large range of estimates for $\delta^{18}O_{ice}$ for the Oligocene (Bohaty et al., 2012b; Lear et al., 2008). It should be noted that the range presented in the climate model are on the lower end of the ice volume estimates as the higher surface topography may have led to a larger ice sheet growth at the EOT with an estimated ice volume of 33.4×10^6 to 35.9×10^6 km^3 (Wilson et al., 2013). Despite the relatively small Oligocene ice sheets in the model, climate model comparisons (ice-no ice) yield too large a cooling with a decrease of -40°C in the middle of the continent (-47 to +7°C temperature change elsewhere). Likely the ice sheet contrast imposed is too great (**Figure S4**), and the problem may lie with the representation of the late Eocene.

The late Eocene included ephemeral glaciations notably the Priabonian Oxygen Isotope Maximum (PrOM) around ~37.5 Ma reaching the coastline, but not persisting (Scher et al., 2014), with glacial initiation in the Gamburtsev Mountains during the latest Eocene (Rose et al., 2013) and glacial erosion before the EOT (Carter et al., 2017; Galeotti et al., 2016). Geochemical evidence from the Kerguelen Plateau at 33.9-33.6 Ma (Scher et al., 2011), and sedimentary records from the western Ross Sea suggest the EOT glacial expansion reached the coast at 32.8 Ma (Galeotti et al., 2016). Modeling ice sheet growth found ephemeral glaciation when pCO_2 reached a threshold of 750-900 ppm (Van Breedam et al., 2022), these pCO_2 levels were reached during the late Eocene as far as back as 40 Ma based on pCO_2 reconstructions (**Figure 1f**) (Rae et al., 2021). Therefore, the lack of ice present in the late Eocene model runs does not match the available evidence for ephemeral ice in Antarctica and may contribute to the proxy-model temperature discrepancies for the individual timeslices.

After the EOT, the use of a full ice sheet for model outputs for the Oligocene is not consistent with pollen evidence for refugial vegetation on the Antarctic Peninsula (Anderson et al., 2011). Proxies record MAT above freezing in the Oligocene and the very presence of plants and soils bacteria indicates that an ice sheet did not cover the entire continent. The mismatch between reconstructed ice and the modelled ice/no ice scenario explains the large proxy-model RMSE for the EOT MATs (**Figure 4**). We would also like to note that the ice sheet extent affects catchment sourcing. In this study, we defined source areas with basic polygons on the continent to represent the catchment area from which terrestrial proxies (e.g., soil biomarkers and rock weathering proxies) are exported to marginal marine settings. With the presence of a large ice sheet, soil and plant derived temperature proxies would be limited to unglaciated areas. However, detailed spatial ice sheet reconstructions are unavailable. Thus, for the purposes of this comparison, the source areas were chosen based on drainage basin, proxy type, and estimated ice sheet extent for the model runs.

4.3. Declining *p*CO_2

Based on the proxy-model comparison it is clear that the lowest RMSE for the Eocene occurs at higher *p*CO_2 (>560 ppmv) which is in line with previous estimates of *p*CO_2 suggesting a late Eocene *p*CO_2 of 830 to 980ppmv from boron and alkenone isotopes (Rae et al., 2021). Previous global proxy model comparison suggest a 40% decrease in *p*CO_2 across the EOT (Hutchinson et al., 2021), attributed to the lack of dynamic ice sheets and under sensitivity to CO_2 forcing (Hutchinson et al., 2021). The absolute *p*CO_2 levels are uncertain in the past, due to factors such as boron isotope seawater uncertainties; however, the boron isotope is better at assessing relative change (Raitzsch & Hönisch, 2013). The boron and alkenone isotopes are well studied for the EOT and have a high amount of data relative to other *p*CO_2 proxies. Current estimates of EOT *p*CO_2 changes from alkenone $\delta^{13}C$ and boron isotopes suggest a decrease of 140 to 150 ppmv, or roughly 25% (Rae et al., 2021). The best fits between the proxies and model runs for the change in temperature, both MAT and SST, and across all the models (**Table S1 and Figure 5**) suggest a 19-30% decrease in *p*CO_2 for MAT and 21-46% decrease for SST after exclusion of Site 511 BAYSPLINE. The percent decrease is higher than previous *p*CO_2 proxy estimates of 16% decrease from boron isotopes (Anagnostou et al., 2016, 2020; Henehan et al., 2020; Pearson et al., 2009) but similar to the estimated 27% decreases from alkenones (Pagani et al., 2005, 2011). The total amount (200-243 ppmv) from the proxy-model comparison is within plausible range of proxy uncertainties. Given that the prescribed post-EOT level was 560 ppmv for the calculations the total amount may vary;

however, the percent change is more comparable to pCO_2 records. The pCO_2 range falls within estimate from pCO_2 proxies. The discrepancy between the scaling and pCO_2 proxies could be due to additional forcing from ice-albedo feedbacks associated with the presence of an ice sheet, sea ice (both likely) and/or changes in paleogeography.

4.4. Paleogeography with declining pCO_2

While the proxy evidence for SST change fits the expected pCO_2 forcing across the Antarctic region, paleogeography could additionally affect regional patterns of cooling. To evaluate the effects of ocean gateways we used the three models with large paleogeographic changes (UViC, CESM_H and FOAM) to derive a temperature anomaly, denoted T_{GEOG}. Note, that T_{GEOG} is calculate from individual models only, not an ensemble of the three models. For each model (UViC, CESM_H and FOAM), we combined this anomaly with the temperature anomaly due to pCO_2 forcing (**Figure S11a**) from the whole ensemble, denoted T_{CO2}, and used adjustable scaling factors α to find a temperature anomaly ΔT to best fit to the proxy data:

$$\Delta T = \alpha(T_{CO2} + T_{GEOG}) \quad (2)$$

By scaling α, we derive a decrease in pCO_2 needed to best fit the proxy data (**Figure S11b, c, d, Table S4**). We excluded alkenone data from Site 511 which was anomalously cold as previously noted. The UViC model pre-EOT run has both the Drake Passage and Tasman Gateway closed while in the post-EOT run both the Drake Passage and Tasman Gateway are open. The CESM_H run model has the Tasman Gateway open post-EOT while the FOAM run models changes the surface area of West Antarctica. With the addition of the UViC model the model ensemble mean pCO_2 decrease needed is 19.9% with an RMSE of 1.66°C. With the inclusion of CESM_H, the decrease in pCO_2 is 30.3% with an RMSE of 1.0°C. With the inclusion of FOAM, the decrease in pCO_2 is 23.2% with an RMSE of 0.95°C. The inclusion of the paleogeographic runs increases the ΔRMSE from 0.0 to ~0.7°C, which is not significant. However, there is a clear change in the rescaled experiments in the amount of pCO_2 needed to drive the transition. The lower pCO_2 decrease, needed for the EOT with these model simulations, is consistent with the theory that the gateways opening around Antarctica were part of the explanation for the changes in regional SSTs.

4.5. Implications for future work

4.5.1. Additional southern hemisphere proxy records

The proxy-model temperature comparison identifies the need for an increase in proxy data spatial coverage for the following reasons: to further constrain the uncertainties on the magnitude of the EOT change, to assess proxy-proxy discrepancies, and to identify how paleogeography drives SST heterogeneity in the Southern Ocean. In the EOT proxy-model comparison we acknowledge a limited number of SST and MAT proxy sites n=6) in the high southern latitudes with most of the records clustered within a few regions. These limited spatial coverage affects the uncertainty and proxy-model comparisons could be more robustly tested with additional sites with proxy reconstructions. On the continent, the availability of additional archives is limited to sites with accessible, outcropping sediments of suitable age, and the modern ice cover is the main impediment. Geological field prospecting for available sediments is the way to see what is possible in terms of adding more MAT estimates and a model-based approach would not be very fruitful to guide land sampling given accessibility limitations, although might help with prioritizing marine margin sites for terrestrial reconstruction. In the open oceans, sediment is in theory deposited everywhere, though water depth and other conditions do limit the availability of SST proxies in some instances (whether through production or preservation). However, there remains great potential to add spatial coverage to proxy SST data and evaluate whether additional proxy records would decrease the proxy-model RMSE. Climate model experiments can help to target marine sampling efforts including guides to the optimal number and locations to drill. Here we demonstrated how an increasing number of sites can reduce the uncertainty of proxy-model SST comparison RMSE, in **Section 4.1.** Beyond the high latitude focus of this study, there is also a dearth of proxy data across the southern hemisphere (especially 20-50ºS) and Hutchinson et al., (2021), called for more southern hemisphere coverage to enable reconstructions and model comparisons of continental climate and changes in ocean temperature and circulation.

4.5.2. Reducing model discrepancy

While sparse proxy data contrasts with the global coverage of climate modelled data, and visibly limits proxy-model temperature comparisons, the lack of improvement when performing synthetic comparisons using additional grid cells for the model inter-comparison reveals that model-model disagreement is the major limiting factor in proxy-model comparisons. While additional proxy records would increase the density of evidence for past climates, and these additional proxy data may improve the robustness of proxy-proxy comparisons, this is not the main driver of the uncertainty (RMSE) in proxy-model comparisons at present. Our analysis identifies the primary source of uncertainty is within the model ensemble. The priority for future work is to address discrepancies in the temperature estimates among the model ensemble as well as the uncertainty surrounding estimation of the $p\mathrm{CO_2}$ decrease needed to force the climate transition of the EOT.

5 Conclusions

The synthesis of recent paleoenvironmental proxy evidence from the high southern latitudes and detailed comparison to regional patterns in climate model experiments allows a new perspective on Antarctic-proximal changes across the EOT. We find spatially heterogeneous cooling of 0 to 3°C (SSTs) and 0 to 4°C (MAT) on land. However, no data are available for the late Eocene and early Oligocene from the Bellingshausen and Amundsen Seas, or adjacent landmasses. Climate model experiments with prescribed ice sheets lead to localized cooling exceeding that recorded by Oligocene proxies. Our comparison supports higher $p\mathrm{CO_2}$ estimates (>800 ppmv) for the late Eocene to match late Eocene temperature proxies. We compared proxy records to model outputs that assessed a decline in $p\mathrm{CO_2}$, changes in paleogeography, and the addition of a near or above modern size ice sheet. We use these various model experiments to estimate the decline in $p\mathrm{CO_2}$ across the transition that provides the best fit to proxy records from the Antarctic across the Eocene-Oligocene Transition. The decline in MAT and SST from the new proxy compilation was used to scale the multi-model ensemble suggesting a 30 to 33% decrease in pCO_2 similar to recent pCO_2 compilations (Rae et al., 2021). This is encouraging as it suggests that the proxy and climate model data on temperature, pCO_2 and sensitivity may be converging on the magnitude of the pCO_2 forcing of the EOT. However, we caution that inter-model divergence remains the largest source of uncertainty in proxy-model comparisons.

Acknowledgements

We declare no financial conflicts of interests for any author or their affiliations. This research was funded by the U.S. National Science Foundation AGS-1844380 to NJB and OPP-1908548 to SJF. This work resulted from the GeoMeetsClimate MIP internship for EJT at GMU directed by NJB. DKH was supported by ARC grant DE220100279. Thanks to Scott Knapp for technical assistance to EJT with coding. Thanks to the various modeling and proxy groups that had made their data publicly accessible or fulfilled requests for data or metadata.

Open Research

The proxy compilation is available at Zenodo (Tibbett et al., 2022a). The code notebooks used to perform the analysis and make the figures are available on GitHub (Tibbett et al., 2022d).

References

Amoo, M., Salzmann, U., Pound, M. J., Thompson, N., & Bijl, P. K. (2022). Eocene to Oligocene vegetation and climate in the Tasmanian Gateway region were controlled by changes in ocean currents and pCO_2. *Climate of the Past*, *18*(3), 525–546. https://doi.org/10.5194/cp-18-525-2022

Anagnostou, E., John, E. H., Babila, T. L., Sexton, P. F., Ridgwell, A., Lunt, D. J., Pearson, P. N., Chalk, T. B., Pancost, R. D., & Foster, G. L. (2020). Proxy evidence for state-dependence of climate sensitivity in the Eocene greenhouse. *Nature Communications*, *11*(1), 4436. https://doi.org/10.1038/s41467-020-17887-x

Anagnostou, E., John, E. H., Edgar, K. M., Foster, G. L., Ridgwell, A., Inglis, G. N., Pancost, R. D., Lunt, D. J., & Pearson, P. N. (2016). Changing atmospheric CO2 concentration was the primary driver of early Cenozoic climate. *Nature*, *533*, 380.

Baatsen, M., von der Heydt, A. S., Huber, M., Kliphuis, M. A., Bijl, P. K., Sluijs, A., & Dijkstra, H. A. (2020). The middle-to-late Eocene greenhouse climate, modelled using the CESM 1.0.5. *Climate of the Past Discussions*, *2020*, 1–44. https://doi.org/10.5194/cp-2020-29

Bohaty, S. M., Zachos, J. C., & Delaney, M. L. (2012a). Foraminiferal Mg/Ca evidence for Southern Ocean cooling across the Eocene–Oligocene transition. *Earth and Planetary Science Letters*, *317–318*, 251–261. https://doi.org/10.1016/j.epsl.2011.11.037

Bohaty, S. M., Zachos, J. C., & Delaney, M. L. (2012b). Foraminiferal Mg/Ca evidence for Southern Ocean cooling across the Eocene-Oligocene transition. *Earth and Planetary Science Letters*, *317*, 251–261. https://doi.org/10.1016/j.epsl.2011.11.037

Carter, A., Riley, T. R., Hillenbrand, C.-D., & Rittner, M. (2017). Widespread Antarctic glaciation during the Late Eocene. *Earth and Planetary Science Letters*, *458*, 49–57. https://doi.org/10.1016/j.epsl.2016.10.045

Coxall, H. K., Huck, C. E., Huber, M., Lear, C. H., Legarda-Lisarri, A., O'Regan, M., Sliwinska, K. K., van de Flierdt, T., de Boer, A. M., Zachos, J. C., & Backman, J. (2018). Export of nutrient rich Northern Component Water preceded early Oligocene Antarctic glaciation. *Nature Geoscience*, *11*(3), 190–196. https://doi.org/10.1038/s41561-018-0069-9

Coxall, H. K., & Pearson, P. N. (2007). The Eocene-Oligocene transition. *Deep Time Perspectives on Climate Change: Marrying the Signal From Computer Models and Biological Proxies*, 351–387.

Coxall, H. K., Wilson, P. A., Palike, H., Lear, C. H., & Backman, J. (2005). Rapid stepwise onset of Antarctic glaciation and deeper calcite compensation in the Pacific Ocean. *Nature*, *433*(7021), 53–57. https://doi.org/10.1038/nature03135

Dalziel, I. W. D., Lawver, L. A., Pearce, J. A., Barker, P. F., Hastie, A. R., Barfod, D. N., Schenke, H.-W., & Davis, M. B. (2013). A potential barrier to deep Antarctic circumpolar flow until the late Miocene? *Geology*, *41*(9), 947–950. https://doi.org/10.1130/G34352.1

De Jonge, C., Hopmans, E. C., Zell, C. I., Kim, J.-H., Schouten, S., & Sinninghe Damsté, J. S. (2014). Occurrence and abundance of 6-methyl branched glycerol dialkyl glycerol tetraethers in soils: Implications for palaeoclimate reconstruction. *Geochimica et Cosmochimica Acta*, *141*, 97–112. https://doi.org/10.1016/j.gca.2014.06.013

Dearing Crampton-Flood, E., Tierney, J. E., Peterse, F., Kirkels, F. M. S. A., & Sinninghe Damsté, J. S. (2020). BayMBT: A Bayesian calibration model for branched glycerol dialkyl glycerol tetraethers in soils and peats. *Geochimica et Cosmochimica Acta*, *268*, 142–159. https://doi.org/10.1016/j.gca.2019.09.043

DeConto, R. M., & Pollard, D. (2003). Rapid Cenozoic glaciation of Antarctica induced by declining atmospheric CO2. *Nature*, *421*(6920), 245–249. https://doi.org/10.1038/nature01290

Deng, L., Jia, G., Jin, C., & Li, S. (2016). Warm season bias of branched GDGT temperature estimates causes underestimation of altitudinal lapse rate. *Organic Geochemistry*, *96*, 11–17. https://doi.org/10.1016/j.orggeochem.2016.03.004

Douglas, P. M. J., Affek, H. P., Ivany, L. C., Houben, A. J. P., Sijp, W. P., Sluijs, A., Schouten, S., & Pagani, M. (2014). Pronounced zonal heterogeneity in Eocene southern high-latitude sea surface temperatures. *Proceedings of the National Academy of Sciences*, *111*(18), 6582. https://doi.org/10.1073/pnas.1321441111

Elsworth, G., Galbraith, E., Halverson, G., & Yang, S. (2017). Enhanced weathering and CO2 drawdown caused by latest Eocene strengthening of the Atlantic meridional overturning circulation. *Nature Geoscience*, *10*(3), 213–216. https://doi.org/10.1038/ngeo2888

Francis, J. E., Marenssi, S., Levy, R., Hambrey, M., Thorn, V. C., Mohr, B., Brinkhuis, H., Warnaar, J., Zachos, J., Bohaty, S., & DeConto, R. (2008). Chapter 8 From Greenhouse to Icehouse – The Eocene/Oligocene in Antarctica. In F. Florindo & M. Siegert (Eds.), *Developments in Earth and*

Environmental Sciences (Vol. 8, pp. 309–368). Elsevier. https://doi.org/10.1016/S1571-9197(08)00008-6

Fyke, J. G., D'Orgeville, M., & Weaver, A. J. (2015). Drake Passage and Central American Seaway controls on the distribution of the oceanic carbon reservoir. *Global and Planetary Change*, *128*, 72–82. https://doi.org/10.1016/j.gloplacha.2015.02.011

Galeotti, S., DeConto, R., Naish, T., Stocchi, P., Florindo, F., Pagani, M., Barrett, P., Bohaty, S. M., Lanci, L., Pollard, D., Sandroni, S., Talarico, F. M., & Zachos, J. C. (2016). Antarctic Ice Sheet variability across the Eocene-Oligocene boundary climate transition. *Science*, *352*(6281), 76. https://doi.org/10.1126/science.aab0669

Ghosh, P., Adkins, J., Affek, H., Balta, B., Guo, W., Schauble, E. A., Schrag, D., & Eiler, J. M. (2006). 13C–18O bonds in carbonate minerals: A new kind of paleothermometer. *Geochimica et Cosmochimica Acta*, *70*(6), 1439–1456. https://doi.org/10.1016/j.gca.2005.11.014

Goldner, A., Herold, N., & Huber, M. (2014). Antarctic glaciation caused ocean circulation changes at the Eocene–Oligocene transition. *Nature*, *511*(7511), 574–577. https://doi.org/10.1038/nature13597

Gradstein, F. M., Ogg, J. G., Schmitz, M. B., & Ogg, G. M. (2012). *The geologic time scale 2012*. elsevier.

Harbert, R. S., & Nixon, K. C. (2015). Climate reconstruction analysis using coexistence likelihood estimation (CRACLE): A method for the estimation of climate using vegetation. *American Journal of Botany*, *102*(8), 1277–1289. https://doi.org/10.3732/ajb.1400500

Hartman, J. D., Sangiorgi, F., Salabarnada, A., Peterse, F., Houben, A. J. P., Schouten, S., Brinkhuis, H., Escutia, C., & Bijl, P. K. (2018). Paleoceanography and ice sheet variability offshore Wilkes Land, Antarctica – Part 3: Insights from Oligocene–Miocene TEX_{86}-based sea surface temperature reconstructions. *Climate of the Past*, *14*(9), 1275–1297. https://doi.org/10.5194/cp-14-1275-2018

Henderiks, J., & Pagani, M. (2008). Coccolithophore cell size and the Paleogene decline in atmospheric CO2. *Earth and Planetary Science Letters*, *269*(3), 576–584. https://doi.org/10.1016/j.epsl.2008.03.016

Henehan, M. J., Edgar, K. M., Foster, G. L., Penman, D. E., Hull, P. M., Greenop, R., Anagnostou, E., & Pearson, P. N. (2020). Revisiting the Middle Eocene Climatic Optimum "Carbon Cycle Conundrum" with new estimates of atmospheric pCO2 from boron isotopes. *Paleoceanography and Paleoclimatology*, *35*(6), e2019PA003713.

Hollis, C. J., Dunkley Jones, T., Anagnostou, E., Bijl, P. K., Cramwinckel, M. J., Cui, Y., Dickens, G. R., Edgar, K. M., Eley, Y., Evans, D., Foster, G. L., Frieling, J., Inglis, G. N., Kennedy, E. M., Kozdon, R., Lauretano, V., Lear, C. H., Littler, K., Lourens, L., … Lunt, D. J. (2019). The DeepMIP contribution to PMIP4: Methodologies for selection, compilation and analysis of latest Paleocene and early Eocene climate proxy data, incorporating version 0.1 of the DeepMIP database. *Geoscientific Model Development*, *12*(7), 3149–3206. https://doi.org/10.5194/gmd-12-3149-2019

Hopmans, E. C., Schouten, S., & Sinninghe Damsté, J. S. (2016). The effect of improved chromatography on GDGT-based palaeoproxies. *Organic Geochemistry*, *93*, 1–6. https://doi.org/10.1016/j.orggeochem.2015.12.006

Houben, A. J. P., Bijl, P. K., Sluijs, A., Schouten, S., & Brinkhuis, H. (2019). Late Eocene Southern Ocean Cooling and Invigoration of Circulation Preconditioned Antarctica for Full-Scale Glaciation. *Geochemistry, Geophysics, Geosystems*, *20*(5), 2214–2234. https://doi.org/10.1029/2019GC008182

Houben, A. J. P., van Mourik, C. A., Montanari, A., Coccioni, R., & Brinkhuis, H. (2012). The Eocene–Oligocene transition: Changes in sea level, temperature or both? *Cenozoic Evolution of Antarctic Climates, Oceans and Ice Sheets*, *335–336*, 75–83. https://doi.org/10.1016/j.palaeo.2011.04.008

Hunt, R. J., & Poole, I. (2003). *Paleogene West Antarctic climate and vegetation history in light of new data from King George Island*.

Hutchinson, D. K., Coxall, H. K., Lunt, D. J., Steinthorsdottir, M., de Boer, A. M., Baatsen, M., von der Heydt, A., Huber, M., Kennedy-Asser, A. T., Kunzmann, L., Ladant, J.-B., Lear, C. H., Moraweck, K., Pearson, P. N., Piga, E., Pound, M. J., Salzmann, U., Scher, H. D., Sijp, W. P., … Zhang, Z. (2021). The Eocene–Oligocene transition: A review of marine and terrestrial proxy data, models and model–data comparisons. *Climate of the Past*, *17*(1), 269–315. https://doi.org/10.5194/cp-17-269-2021

Hutchinson, D. K., Coxall, H. K., O′Regan, M., Nilsson, J., Caballero, R., & de Boer, A. M. (2019). Arctic closure as a trigger for Atlantic overturning at the Eocene-Oligocene Transition. *Nature Communications*, *10*(1), 3797. https://doi.org/10.1038/s41467-019-11828-z

Hutchinson, D. K., de Boer, A. M., Coxall, H. K., Caballero, R., Nilsson, J., & Baatsen, M. (2018). Climate sensitivity and meridional overturning circulation in the late Eocene using GFDL CM2.1. *Clim. Past*, *14*(6), 789–810. https://doi.org/10.5194/cp-14-789-2018

Kalanetra, K. M., Bano, N., & Hollibaugh, J. T. (2009). Ammonia-oxidizing Archaea in the Arctic Ocean and Antarctic coastal waters. *Environmental Microbiology*, *11*(9), 2434–2445.

Katz, M. E., Miller, K. G., Wright, J. D., Wade, B. S., Browning, J. V., Cramer, B. S., & Rosenthal, Y. (2008). Stepwise transition from the Eocene greenhouse to the Oligocene icehouse. *Nature Geoscience*, *1*(5), 329–334. https://doi.org/10.1038/ngeo179

Kennedy, A. T., Farnsworth, A., Lunt, D. J., Lear, C. H., & Markwick, P. J. (2015). Atmospheric and oceanic impacts of Antarctic glaciation across the Eocene–Oligocene transition. *Philosophical Transactions of the Royal Society A: Mathematical, Physical and Engineering Sciences*, *373*(2054), 20140419. https://doi.org/10.1098/rsta.2014.0419

Kennedy-Asser, A. T., Lunt, D. J., Valdes, P. J., Ladant, J.-B., Frieling, J., & Lauretano, V. (2020). Changes in the high-latitude Southern Hemisphere through the Eocene–Oligocene transition: A model–data comparison. *Climate of the Past*, *16*(2), 555–573. https://doi.org/10.5194/cp-16-555-2020

Kennett, J. P. (1977). Cenozoic evolution of Antarctic glaciation, the circum-Antarctic Ocean, and their impact on global paleoceanography. *Journal of Geophysical Research (1896-1977)*, *82*(27), 3843–3860. https://doi.org/10.1029/JC082i027p03843

Ladant, J. B., Donnadieu, Y., & Dumas, C. (2014). Links between CO2, glaciation and water flow: Reconciling the Cenozoic history of the Antarctic Circumpolar Current. *Clim. Past*, *10*(6), 1957–1966. https://doi.org/10.5194/cp-10-1957-2014

Ladant, J.-B., Donnadieu, Y., Lefebvre, V., & Dumas, C. (2014). The respective role of atmospheric carbon dioxide and orbital parameters on ice sheet evolution at the Eocene-Oligocene transition. *Paleoceanography*, *29*(8), 810–823. https://doi.org/10.1002/2013PA002593

Lauretano, V., Kennedy-Asser, A. T., Korasidis, V. A., Wallace, M. W., Valdes, P. J., Lunt, D. J., Pancost, R. D., & Naafs, B. D. A. (2021). Eocene to Oligocene terrestrial Southern Hemisphere cooling caused by declining pCO2. *Nature Geoscience*, *14*(9), 659–664. https://doi.org/10.1038/s41561-021-00788-z

Lear, C. H., Bailey, T. R., Pearson, P. N., Coxall, H. K., & Rosenthal, Y. (2008). Cooling and ice growth across the Eocene-Oligocene transition. *Geology*, *36*(3), 251–254. https://doi.org/10.1130/G24584A.1

Liu, Z., Pagani, M., Zinniker, D., DeConto, R., Huber, M., Brinkhuis, H., Shah, S. R., Leckie, R. M., & Pearson, A. (2009). Global Cooling During the Eocene-Oligocene Climate Transition. *Science*, *323*(5918), 1187. https://doi.org/10.1126/science.1166368

M. McKay, R., Escutia, C., De Santis, L., Donda, F., Duncan, B., Gohl, K., Gulick, S., Hernández-Molina, J., Hillenbrand, C.-D., Hochmuth, K., Kim, S., Kuhn, G., Larter, R., Leitchenkov, G., H. Levy, R., R. Naish, T., O’Brien, P., F. Pérez, L., E. Shevenell, A., & Williams, T. (2022). Chapter 3—Cenozoic history of Antarctic glaciation and climate from onshore and offshore studies. In F. Florindo, M. Siegert, L. D. Santis, & T. Naish (Eds.), *Antarctic Climate Evolution (Second Edition)* (pp. 41–164). Elsevier. https://doi.org/10.1016/B978-0-12-819109-5.00008-6

Macphail, M. K., & Truswell, E. M. (2004). Palynology of Neogene slope and rise deposits from ODP Sites 1165 and 1167, East Antarctica. *Proceedings of the Ocean Drilling Program. Scientific Results*, *188*, 1–20.

Miller, K. G., Browning, J. V., Schmelz, W. J., Kopp, R. E., Mountain, G. S., & Wright, J. D. (2020). Cenozoic sea-level and cryospheric evolution from deep-sea geochemical and continental margin records. *Science Advances*, *6*(20), eaaz1346. https://doi.org/10.1126/sciadv.aaz1346

Müller, R. D., Cannon, J., Qin, X., Watson, R. J., Gurnis, M., Williams, S., Pfaffelmoser, T., Seton, M., Russell, S. H. J., & Zahirovic, S. (2018). GPlates: Building a Virtual Earth Through Deep Time. *Geochemistry, Geophysics, Geosystems*, *19*(7), 2243–2261. https://doi.org/10.1029/2018GC007584

Naafs, B. D. A., Inglis, G. N., Zheng, Y., Amesbury, M. J., Biester, H., Bindler, R., Blewett, J., Burrows, M. A., del Castillo Torres, D., Chambers, F. M., Cohen, A. D., Evershed, R. P., Feakins, S. J., Gałka, M., Gallego-Sala, A., Gandois, L., Gray, D. M., Hatcher, P. G., Honorio Coronado, E. N., … Pancost, R. D. (2017). Introducing global peat-specific temperature and pH calibrations based on brGDGT bacterial lipids. *Geochimica et Cosmochimica Acta*, *208*, 285–301. https://doi.org/10.1016/j.gca.2017.01.038

Pagani, M., Huber, M., Liu, Z., Bohaty, S. M., Henderiks, J., Sijp, W., Krishnan, S., & DeConto, R. M. (2011). The Role of Carbon Dioxide During the Onset of Antarctic Glaciation. *Science*, *334*(6060), 1261. https://doi.org/10.1126/science.1203909

Pagani, M., Zachos, J. C., Freeman, K. H., Tipple, B., & Bohaty, S. (2005). Marked Decline in Atmospheric Carbon Dioxide Concentrations During the Paleogene. *Science*, *309*(5734), 600. https://doi.org/10.1126/science.1110063

Passchier, S., Bohaty, S. M., Jimenez-Espejo, F. J., Pross, J., Roehl, U., van de Flierdt, T., Escutia, C., & Brinkhuis, H. (2013). Early Eocene to middle Miocene cooling and aridification of East Antarctica. *Geochemistry Geophysics Geosystems*, *14*(5), 1399–1410. https://doi.org/10.1002/ggge.20106

Passchier, S., Ciarletta, D. J., Miriagos, T. E., Bijl, P. K., & Bohaty, S. M. (2017). An Antarctic stratigraphic record of stepwise ice growth through the Eocene-Oligocene transition. *Geological Society of America Bulletin*, *129*(3–4), 318–330. https://doi.org/10.1130/B31482.1

Paxman, G. J. G., Jamieson, S. S. R., Ferraccioli, F., Bentley, M. J., Ross, N., Armadillo, E., Gasson, E. G. W., Leitchenkov, G., & DeConto, R. M. (2018). Bedrock Erosion Surfaces Record Former East Antarctic Ice Sheet Extent. *Geophysical Research Letters*, *45*(9), 4114–4123. https://doi.org/10.1029/2018GL077268

Paxman, G. J. G., Jamieson, S. S. R., Hochmuth, K., Gohl, K., Bentley, M. J., Leitchenkov, G., & Ferraccioli, F. (2019). Reconstructions of Antarctic topography since the Eocene–Oligocene boundary. *Palaeogeography, Palaeoclimatology, Palaeoecology*, *535*, 109346. https://doi.org/10.1016/j.palaeo.2019.109346

Pearson, P. N., Foster, G. L., & Wade, B. S. (2009). Atmospheric carbon dioxide through the Eocene–Oligocene climate transition. *Nature*, *461*(7267), 1110–1113. https://doi.org/10.1038/nature08447

Petersen, S. V., & Schrag, D. P. (2015). Antarctic ice growth before and after the Eocene-Oligocene transition: New estimates from clumped isotope paleothermometry: Antarctic ice growth at the E/O transition. *Paleoceanography*, *30*(10), 1305–1317. https://doi.org/10.1002/2014PA002769

Plancq, J., Mattioli, E., Pittet, B., Simon, L., & Grossi, V. (2014). Productivity and sea-surface temperature changes recorded during the late Eocene–early Oligocene at DSDP Site 511 (South Atlantic). *Palaeogeography, Palaeoclimatology, Palaeoecology*, *407*, 34–44. https://doi.org/10.1016/j.palaeo.2014.04.016

Poole, I., Cantrill, D., & Utescher, T. (2005). A multi-proxy approach to determine Antarctic terrestrial palaeoclimate during the Late Cretaceous and Early Tertiary. *Palaeogeography, Palaeoclimatology, Palaeoecology*, *222*(1), 95–121. https://doi.org/10.1016/j.palaeo.2005.03.011

Popp, B. N., Prahl, F. G., Wallsgrove, R. J., & Tanimoto, J. (2006). Seasonal patterns of alkenone production in the subtropical oligotrophic North Pacific. *Paleoceanography*, *21*(1). Scopus. https://doi.org/10.1029/2005PA001165

Pound, M. J., & Salzmann, U. (2017). Heterogeneity in global vegetation and terrestrial climate change during the late Eocene to early Oligocene transition. *Scientific Reports*, *7*, 43386. https://doi.org/10.1038/srep43386

Prahl, F. G., & Wakeham, S. G. (1987). Calibration of unsaturation patterns in long-chain ketone compositions for palaeotemperature assessment. *Nature*, *330*(6146), 367–369. https://doi.org/10.1038/330367a0

Rae, J. W. B., Zhang, Y. G., Liu, X., Foster, G. L., Stoll, H. M., & Whiteford, R. D. M. (2021). Atmospheric CO2 over the Past 66 Million Years from Marine Archives. *Annual Review of Earth and Planetary Sciences*, *49*(1), 609–641. https://doi.org/10.1146/annurev-earth-082420-063026

Raitzsch, M., & Hönisch, B. (2013). Cenozoic boron isotope variations in benthic foraminifers. *Geology*, *41*(5), 591–594. https://doi.org/10.1130/G34031.1

Rose, K. C., Ferraccioli, F., Jamieson, S. S. R., Bell, R. E., Corr, H., Creyts, T. T., Braaten, D., Jordan, T. A., Fretwell, P. T., & Damaske, D. (2013). Early East Antarctic Ice Sheet growth recorded in the landscape of the Gamburtsev Subglacial Mountains. *Earth and Planetary Science Letters*, *375*, 1–12. https://doi.org/10.1016/j.epsl.2013.03.053

Sauermilch, I., Whittaker, J. M., Klocker, A., Munday, D. R., Hochmuth, K., Bijl, P. K., & LaCasce, J. H. (2021). Gateway-driven weakening of ocean gyres leads to Southern Ocean cooling. *Nature Communications*, *12*(1), 6465. https://doi.org/10.1038/s41467-021-26658-1

Scher, H. D., Bohaty, S. M., Smith, B. W., & Munn, G. H. (2014). Isotopic interrogation of a suspected late Eocene glaciation. *Paleoceanography*, *29*(6), 628–644. https://doi.org/10.1002/2014PA002648

Scher, H. D., Bohaty, S. M., Zachos, J. C., & Delaney, M. L. (2011). Two-stepping into the icehouse: East Antarctic weathering during progressive ice-sheet expansion at the Eocene–Oligocene transition. *Geology*, *39*(4), 383–386. https://doi.org/10.1130/G31726.1

Scher, H. D., Whittaker, J. M., Williams, S. E., Latimer, J. C., Kordesch, W. E. C., & Delaney, M. L. (2015). Onset of Antarctic Circumpolar Current 30 million years ago as Tasmanian Gateway aligned with westerlies. *Nature*, *523*(7562), 580–583. https://doi.org/10.1038/nature14598

Schouten, S., Hopmans, E. C., Schefuß, E., & Damste, J. S. S. (2002). Distributional variations in marine crenarchaeotal membrane lipids: A new tool for reconstructing ancient sea water temperatures? *Earth and Planetary Science Letters*, *204*(1–2), 265–274.

Sheldon, N. D., Retallack, G. J., & Tanaka, S. (2002). Geochemical Climofunctions from North American Soils and Application to Paleosols across the Eocene-Oligocene Boundary in Oregon. *The Journal of Geology*, *110*(6), 687–696. https://doi.org/10.1086/342865

Sheldon, N. D., & Tabor, N. J. (2009). Quantitative paleoenvironmental and paleoclimatic reconstruction using paleosols. *Earth-Science Reviews*, *95*(1), 1–52. https://doi.org/10.1016/j.earscirev.2009.03.004

Sijp, W. P., England, M. H., & Toggweiler, J. R. (2009). Effect of Ocean Gateway Changes under Greenhouse Warmth. *Journal of Climate*, *22*(24), 6639–6652. https://doi.org/10.1175/2009JCLI3003.1

Sijp, W. P., von der Heydt, A. S., & Bijl, P. K. (2016). Model simulations of early westward flow across the Tasman Gateway during the early Eocene. *Clim. Past*, *12*(4), 807–817. https://doi.org/10.5194/cp-12-807-2016

Sikes, E. L., & Volkman, J. K. (1993). Calibration of alkenone unsaturation ratios (Uk'37) for paleotemperature estimation in cold polar waters. *Geochimica et Cosmochimica Acta*, *57*(8), 1883–1889. https://doi.org/10.1016/0016-7037(93)90120-L

Sikes, E. L., Volkman, J. K., Robertson, L. G., & Pichon, J. J. (1997). Alkenones and alkenes in surface waters and sediments of the Southern Ocean: Implications for paleotemperature estimation in polar regions. *Geochimica Et Cosmochimica Acta*, *61*(7), 1495–1505. https://doi.org/10.1016/S0016-7037(97)00017-3

Speelman, E. N., van Kempen, M. M., Barke, J., Brinkhuis, H., Reichart, G.-J., Smolders, A. J., Roelofs, J. G., Sangiorgi, F., de Leeuw, J. W., & Lotter, A. F. (2009). The Eocene Arctic Azolla bloom: Environmental conditions, productivity and carbon drawdown. *Geobiology*, *7*(2), 155–170.

Thompson, N., Salzmann, U., López-Quirós, A., Bijl, P. K., Hoem, F. S., Etourneau, J., Sicre, M.-A., Roignant, S., Hocking, E., Amoo, M., & Escutia, C. (2022). Vegetation change across the Drake Passage region linked to late Eocene cooling and glacial disturbance after the Eocene–Oligocene transition. *Climate of the Past*, *18*(2), 209–232. https://doi.org/10.5194/cp-18-209-2022

Tibbett, E. J., Burls, N. J., Hutchinson, D. K., & Feakins, S. J. (2022d). Ejtibbett/EOTproxymodel: Proxy Model Comparison for the Eocene-Oligocene Transition [ComputationalNotebook]. *Zenodo*. https://doi.org/10.5281/zenodo.7254786

Tibbett, E. J., Burls, N. J., Hutchinson, D. K., & Feakins, S. J. (2022a). Southern High Latitude Temperature Proxies from the Late Eocene and Early Oligocene [Dataset]. *Zenodo*. https://doi.org/10.5281/zenodo.7254536

Tibbett, E. J., Scher, H. D., Warny, S., Tierney, J. E., & Feakins, S. J. (2021b). *Prydz Bay East Antarctica, biomarker and pollen, 36-33 million years. NOAA Paleoclimate Database*. https://www.ncdc.noaa.gov/paleo/study/32052

Tibbett, E. J., Scher, H. D., Warny, S., Tierney, J. E., Passchier, S., & Feakins, S. J. (2021a). Late Eocene Record of Hydrology and Temperature From Prydz Bay, East Antarctica. *Paleoceanography and Paleoclimatology*, *36*(4), e2020PA004204. https://doi.org/10.1029/2020PA004204

Tibbett, E. J., Warny, S., Tierney, J. E., Wellner, J. S., & Feakins, S. J. (2022b). Cenozoic Antarctic Peninsula Temperatures and Glacial Erosion Signals From a Multi-Proxy Biomarker Study. *Paleoceanography and Paleoclimatology*, *37*(9), e2022PA004430. https://doi.org/10.1029/2022PA004430

Tibbett, E. J., Warny, S., Tierney, J. E., Wellner, J. S., & Feakins, S. J. (2022c). SHALDRIL Antarctic Peninsula, biomarkers, 37-3 million years [Dataset]. *NOAA Paleoclimate Database*. https://www.ncdc.noaa.gov/paleo/study/35613

Tierney, J. E., & Tingley, M. P. (2014). A Bayesian, spatially-varying calibration model for the TEX86 proxy. *Geochimica et Cosmochimica Acta*, *127*, 83–106.

Tierney, J. E., & Tingley, M. P. (2018). BAYSPLINE: A New Calibration for the Alkenone Paleothermometer. *Paleoceanography and Paleoclimatology*, *33*(3), 281–301. https://doi.org/10.1002/2017PA003201

Toumoulin, A., Donnadieu, Y., Ladant, J.-B., Batenburg, S. J., Poblete, F., & Dupont-Nivet, G. (2020). Quantifying the Effect of the Drake Passage Opening on the Eocene Ocean. *Paleoceanography and Paleoclimatology*, *35*(8), e2020PA003889. https://doi.org/10.1029/2020PA003889

Truswell, E. M., & Macphail, M. K. (2009). Polar forests on the edge of extinction: What does the fossil spore and pollen evidence from East Antarctica say? *Australian Systematic Botany*, *22*(2), 57–106. https://doi.org/10.1071/SB08046

Utescher, T., Bruch, A. A., Erdei, B., François, L., Ivanov, D., Jacques, F. M. B., Kern, A. K., Liu, Y.-S. (C.), Mosbrugger, V., & Spicer, R. A. (2014). The Coexistence Approach—Theoretical background and practical considerations of using plant fossils for climate quantification. *Palaeogeography, Palaeoclimatology, Palaeoecology*, *410*, 58–73. https://doi.org/10.1016/j.palaeo.2014.05.031

Vahlenkamp, M., Niezgodzki, I., De Vleeschouwer, D., Lohmann, G., Bickert, T., & Pälike, H. (2018). Ocean and climate response to North Atlantic seaway changes at the onset of long-term Eocene cooling. *Earth and Planetary Science Letters*, *498*, 185–195. https://doi.org/10.1016/j.epsl.2018.06.031

Van Breedam, J., Huybrechts, P., & Crucifix, M. (2022). Modelling evidence for late Eocene Antarctic glaciations. *Earth and Planetary Science Letters*, *586*, 117532. https://doi.org/10.1016/j.epsl.2022.117532

Volkman, J. K., Eglinton, G., Corner, E. D. S., & Forsberg, T. E. V. (1980). Long-chain alkenes and alkenones in the marine coccolithophorid Emiliania huxleyi. *Phytochemistry*, *19*(12), 2619–2622. https://doi.org/10.1016/S0031-9422(00)83930-8

Weijers, J. W. H., Bernhardt, B., Peterse, F., Werne, J. P., Dungait, J. A. J., Schouten, S., & Sinninghe Damsté, J. S. (2011). Absence of seasonal patterns in MBT–CBT indices in mid-latitude soils. *Geochimica et Cosmochimica Acta*, *75*(11), 3179–3190. https://doi.org/10.1016/j.gca.2011.03.015

Weijers, J. W. H., Schouten, S., van den Donker, J. C., Hopmans, E. C., & Sinninghe Damsté, J. S. (2007). Environmental controls on bacterial tetraether membrane lipid distribution in soils. *Geochimica et Cosmochimica Acta*, *71*(3), 703–713. https://doi.org/10.1016/j.gca.2006.10.003

Westerhold, T., Marwan, N., Drury, A. J., Liebrand, D., Agnini, C., Anagnostou, E., Barnet, J. S. K., Bohaty, S. M., Vleeschouwer, D. D., Florindo, F., Frederichs, T., Hodell, D. A., Holbourn, A. E., Kroon, D., Lauretano, V., Littler, K., Lourens, L. J., Lyle, M., Pälike, H., … Zachos, J. C. (2020). An astronomically dated record of Earth’s climate and its predictability over the last 66 million years. *Science*, *369*(6509), 1383–1387. https://doi.org/10.1126/science.aba6853

Willard, D. A., Donders, T. H., Reichgelt, T., Greenwood, D. R., Sangiorgi, F., Peterse, F., Nierop, K. G. J., Frieling, J., Schouten, S., & Sluijs, A. (2019). Arctic vegetation, temperature, and hydrology during Early Eocene transient global warming events. *Global and Planetary Change*, *178*, 139–152. https://doi.org/10.1016/j.gloplacha.2019.04.012

Wilson, D. S., Pollard, D., DeConto, R. M., Jamieson, S. S. R., & Luyendyk, B. P. (2013). Initiation of the West Antarctic Ice Sheet and estimates of total Antarctic ice volume in the earliest Oligocene. *Geophysical Research Letters*, *40*(16), 4305–4309. https://doi.org/10.1002/grl.50797

Zhang, Z., Nisancioglu, K., Bentsen, M., Tjiputra, J., Bethke, I., Yan, Q., Risebrobakken, B., Andersson, C., & Jansen, E. (2012). Pre-industrial and mid-Pliocene simulations with NorESM-L. *Geoscientific Model Development*, *5*(2), 523–533. https://doi.org/10.5194/gmd-5-523-2012

Zhang, Z., Ramstein, G., Schuster, M., Li, C., Contoux, C., & Yan, Q. (2014). Aridification of the Sahara desert caused by Tethys Sea shrinkage during the Late Miocene. *Nature*, *513*(7518), 401–404. https://doi.org/10.1038/nature13705

References from the Supporting Information

Baatsen, M., van Hinsbergen, D. J. J., von der Heydt, A. S., Dijkstra, H. A., Sluijs, A., Abels, H. A., & Bijl, P. K. (2016). Reconstructing geographical boundary conditions for palaeoclimate modelling during the Cenozoic. *Climate of the Past*, *12*(8), 1635–1644. https://doi.org/10.5194/cp-12-1635-2016

Scotese, C. (2001). *Digital paleogeographic map archive on CD-ROM. PALEOMAP Project. University of Texas (Arlington)*.

Sewall, J. O., Sloan, L. C., Huber, M., & Wing, S. (2000). Climate sensitivity to changes in land surface characteristics. *Global and Planetary Change*, *26*(4), 445–465. https://doi.org/10.1016/S0921-8181(00)00056-4

Wilson, D. S., Jamieson, S. S. R., Barrett, P. J., Leitchenkov, G., Gohl, K., & Larter, R. D. (2012). Antarctic topography at the Eocene–Oligocene boundary. *Cenozoic Evolution of Antarctic Climates, Oceans and Ice Sheets*, *335–336*, 24–34. https://doi.org/10.1016/j.palaeo.2011.05.028

Paleoceanography and Paleoclimatology

Supporting Information for

Proxy-Model Comparison for the Eocene-Oligocene Transition in Southern High Latitudes

Emily J. Tibbett[1], Natalie J. Burls[2], David K. Hutchinson[3], Sarah J. Feakins[1]

[1]Department of Earth Science, University of Southern California, Los Angeles, CA, USA
[2]Atmospheric, Oceanic, and Earth Sciences Department, George Mason University, Fairfax, VA, USA
[3]Climate Change Research Centre, University of New South Wales, Sydney, Australia

Contents of this file

Introduction

The supporting information associated with the manuscript referenced above includes two supplementary text sections, five supplementary tables and eleven supplementary figures. Text S1 provides background information on the model simulations and text S2 discusses the impact of seasonality on the results. Table S1 contains the RMSE values and calculated pCO_2 decrease. Table S2 compares the RMSE when applying MAT versus MAF from each model. Table S3 reports the RMSE between the proxies and models for both MAT and MAF for each timeslice. Table S4 reports the RMSE and pCO_2 decrease for the paleogeographic runs combined with the ensemble mean. Table S5 reports the RMSE for the inter-model comparison. Table S6 evaluates the impact of the time window averaging for the MAT results and Table S7 does the same for the SST results. Table S8 and S9 provide the results of removing individual proxy records for MAT and SST respectively. Table S10 and S11 evaluate the removal of all records of the same proxy type on the results for MAT and SST respectively. Figure S1 shows the southern hemisphere high latitude MAT for each timeslice. Figure S2 is a detailed map (a zoom in of that mapped on Figure S1) to note localized heterogeneity. Figure S3 southern hemisphere high latitude SSTs. Figure S4 MAT from model runs with and without ice. Figure S5 SST from model runs with and without ice. Figure S6 MAT in paleogeographic model runs. Figure S7 SST in paleogeographic model runs. Figure S8 proxy-model comparison for models scaled to a 25% reduction in pCO_2. Figure S9 model seasonality for each timeslice. Figure S10 compares the best fit pCO_2 scaling for the MAT and MAF comparison. Figure S11 paleogeographic model runs with the model ensemble runs. Figure S12 shows the results of the inter-model comparison using the "perfect model" approach.

Text S1. Model boundary conditions

Here we review the initial grid information for each model from the published literature. For the proxy-model comparison performed here, the models were evaluated on the same uniform grid, that of NorESM-L (Hutchinson et al., 2021). We also summarize key details of each simulation.

CESM-B: Prior to the uniform grid the atmospheric resolution was 144x96x26 and the ocean resolution was 384x320x60 (Baatsen et al., 2020). The low and high pCO_2 experiments come from Baatsen 2020 and 2016 respectively. The spin up was 3600 model years for the low pCO_2 (560 ppm) experiment and 4600 for the high pCO_2 experiment (1120 ppm). The land topography has low resolution which leads to smoothing that underestimates local temperature heterogeneity (Baatsen et al., 2020). The model simulations were in equilibrium for sea surface temperatures and the deep ocean.

CESM-H: The initial resolution was 96x48x26 for the atmosphere with 122x100x25 for the ocean (Goldner et al., 2014). CESM_H contained model simulations that include high and low pCO_2, with and without ice, and changes in paleogeography. For the high (1120ppm) and low (560 ppm) pCO_2 simulations the model was run for 3300 and 3400 model years respectively. For the no ice vs ice simulations, the prescribed pCO_2 was 560 ppm. The prescribed ice volume for the ice simulation was 20.3×10^6 km^3. For the no ice simulation, the model years were 3400 and for the ice simulation the model years were 3000. The paleogeography runs were the closing of the Tasman and Drake Passage (pre-EOT) and opening of both passages (post-EOT) with both simulations using a pCO_2 of 1120ppm. The model years used were 1300 and 1000 model years for both gateways closed and open respectively. The topography on land reflected nearly modern-day levels for the glaciated EOT simulations while the unglaciated EOT simulations used the paleo-elevation reconstruction from Sewall et al., (2000) and discussed potential error introduced by uncertainty in topography. The model was in equilibrium for the deep and surface ocean.

NorESM-L: The initial resolution was 96x48x26 for the atmosphere with 100x116x32 for the ocean (Zhang et al., 2012,2014). The NorESM-L simulations used in this study include low (560 ppm) and high pCO_2 (980 ppm) simulations as well as a simulation with paleogeography changes. The change in pCO_2 between the NorESM-L simulations was not a decrease in pCO_2 of 50%; therefore, to be consistent with the other modelling studies, the high pCO_2 simulation was scaled to 1120ppm to reflect a pCO_2 decrease of 50%. For the paleogeography simulations, the pre-EOT uses the continental configuration of 35 Ma from Scotese et al. (2001) while the post-EOT uses the 33 Ma continental configuration. Both paleogeography simulations were prescribed a pCO_2 of 560 ppm. There are no changes in passageways or changes in the Antarctic continent above/below sea level. For all simulations the model ran for 2200 years.

GFDLCM 2.1: The initial resolution was 96x60x24 for the atmosphere with 240x175x50 for the ocean (Hutchinsons et al., 2018,2019). The GFDLCM 2.1 simulations used were low (400 ppm) vs high (800 ppm) pCO_2 and changes in paleogeography. For the paleogeography changes the pCO_2 was set at 800 ppm for both simulations. The pre-EOT used a 38 Ma reconstruction from Baatsen et al., (2016) while the post-EOT simulation closed the Arctic gateway. All simulations ran for 6500 model years. The topography applied was the 38 Ma reconstruction from Baatsen et al. (2016). The model simulations were determined to be in quasi-equilibrium with the deep ocean gradually cooling (Hutchinson et al., 2018). Although the deep ocean continued to cool, surface temperature and salinity in areas of deep water formation regions were stable along with the overturning circulation (Hutchinson et al., 2019)

FOAM: The initial resolution was 48x40x18 for the atmosphere with 128x128x24 for the ocean (Ladant et al., 2014a,b). The FOAM simulations used here were the low (560 ppm) and high (1120 ppm) pCO_2 runs, no ice vs ice runs, and a run with changes in paleogeography. The ice volume prescribed was 25.0×10^6 km^3. For the paleogeography simulations the pre-EOT was a continental configuration of 34 Ma and post-EOT was 30 Ma. These paleogeography simulations did not include changes in ocean passages/gateways or changes in large areas of Antarctica below or above sea level. All model simulations used 2000 model years. The topography for the model simulations is based on the topography of Antarctica after isostatic adjustment form the removal of the present-day ice sheet (Ladant et al., 2014a). The model simulations used were in equilibrium. In Ladant et al., (2014b) the Antarctic topographic reconstruction is based on that of Wilson et al. (2012) which reconstructed the elevation based on erosion of Antarctica. This leads to a larger area than the isostatically adjusted present day Antarctica topography after removal of the ice sheet (Ladant et al., 2014b).

UViC: The initial resolution was 150x100x11 for the atmosphere with 150x140x0 for the ocean (Sijp et al., 2016). The UviC model simulations used here were for the paleogeography comparison (there were no low and high pCO_2 runs available). The pCO_2 was consistent between runs with a pCO_2 of 1600ppm. The pre-EOT and post-EOT paleogeography was set at 45 Ma (Sewall et al., 2000). For the pre-EOT the Drake passage was closed while in the post-EOT it was open. All simulations were run for 9000 model years. No information was available on the topography. There is also no indication of MAT data from the UviC model in Sijp et al. (2016). The model simulations were run to equilibrium including in the deep ocean (Sijp et al., 2016).

HadCM3BL: The initial resolution was 96x73x19 for the atmosphere with 96x73x20 for the ocean (Kennedy et al., 2015). For HadCM3BL the model simulations used here include low (560 ppm) and high (1120 ppm) for pCO_2, no ice versus ice, and changes in paleogeography. For the no ice and ice runs the pCO_2 was 560ppm for both with a prescribed ice volume of 17.0×10^6 km^3 for the post-EOT ice run. For the paleogeography the pCO_2 was set to 560 ppm. The pre-EOT runs were a continental configuration for the Priabonian and for the post-EOT the Chattian. All model simulations were run for 1422 years. The model simulations were determined to be in quasi-equilibrium as the atmospheric and surface ocean, down to 670 m, are stable.

Text S2. Accounting for proxy seasonality in proxy-model comparisons

To assess the impact of seasonality on the proxy model comparison, we considered a seasonally defined rather than mean annual comparison for land temperature proxies only. For land temperature proxies, both plants and soil bacteria are thought to be summer-active recorders, this motivates an effort to compare to seasonal climate from the models. At this time, however, only $BayMBT_0$ has been explicitly calibrated to MAF, and only one site, Prydz Bay, has MAF estimates for both the Eocene and Oligocene. Using this MAF estimate and the other constraints as before, we compared to the climate model results and recalculated the pCO_2 scaling. The MAF proxy model comparison yields lower RMSE for the individual timeslices (**Figure S8, Table S2**). However, across the EOT the RMSE does not change and yields a similar estimated pCO_2 decrease (**Table S3 and Figure S9**). Although this seasonality proxy-model comparison is limited in application here, it demonstrates the potential for future work to calibrate proxies to seasons and to compare to the seasonal output of climate models in future efforts.

Table S1. Proxy-model discrepancy (as root mean standard error; RMSE) for the MAT and SST proxy-model comparison for the best fit pCO_2 forcing. The proxy constraints are based on n sites where SST proxy n = 6 and MAT proxy n=6. The pCO_2 is expressed in concentration units for the Oligocene-Eocene climate model runs and as a % decrease in the Oligocene relative to the Eocene runs.

	MAT proxy-model comparison			SST proxy-model comparison		
Climate Model	RMSE (°C)	pCO_2 decrease (ppmv)	pCO_2 decrease (%)	RMSE (°C)	pCO_2 decrease (ppmv)	pCO_2 decrease (%)
CESM_B	1.98	129	18.8	0.90	179	33.1
CESM_H	1.68	221	28.3	0.92	221	35.8
GFDLCM 2.1	1.35	200	26.3	1.02	111	21.0
HadCM3BL	2.24	169	23.2	1.23	362	46.4
FOAM	1.58	232	29.3	1.07	159	27.3
NorESM-L	2.34	66	10.5	1.45	375	43.4
Ensemble	**1.88**	**243**	**30.3**	**1.01**	**200**	**33.1**

Table S2. Proxy-model discrepancy (as root mean standard error; RMSE) for land surface air temperature estimates for both the Eocene and Oligocene timeslices, and EOT (Oligocene-Eocene) difference for mean annual surface air temperature (MAT) and months above freezing (MAF). MAF were selected in model runs based on their seasonal climatology. The *br*GDGT calibrations include both MAT and MAF formal calibrations and both are available for Prydz Bay and are used as defined. The other proxies are maintained with their same temperature conversions for both scenarios in order to assess whether they better approximate mean annual or 'summer' (above freezing) conditions. As hypothesized, we find greater agreement in the MAF comparison.

Model Run	Eocene		Oligocene		EOT	
	MAT RMSE (°C)	MAF RMSE (°C)	MAT RMSE (°C)	MAF RMSE (°C)	MAT RMSE (°C)	MAF RMSE (°C)
CESM_B	4.6	4.5	5.7	5.1	3.6	2.4
CESM_H	4.6	3.8	5.6	4.6	2.5	2.4
GFDL CM2.1	4.6	3.1	5.7	3.6	2.8	2.6
HadCM3BL	8.0	3.8	6.8	3.8	2.5	1.8
FOAM	6.1	4.0	7.3	4.3	2.4	1.8
NorESM-L	7.5	3.7	5.7	3.2	3.1	1.9
Ensemble	**5.2**	**3.2**	**5.0**	**3.4**	**2.3**	**2.1**

Table S3. Estimated pCO_2 decrease across the EOT for scaling experiments based on land surface air temperatures comparison results of the MAT and MAF* model outputs and proxy** comparisons. Only Prydz Bay had proxy data for both the Eocene and Oligocene as MAF formally derived, all other proxy data were unchanged from the MAT case, but many may have warm-season recording bias

Model Run	MAT		MAF	
	pCO_2 decrease (%)	pCO_2 decrease (ppmv)	pCO_2 decrease (%)	pCO_2 decrease (ppmv)
CESM_B	18.8	129	27.3	210
CESM_H	28.3	221	26.3	200
GFDL CM2.1	26.3	200	24.2	179
HadCM3BL	23.2	169	33.1	277
FOAM	29.3	232	35.8	313
NorESM-L	10.5	66	31.2	254
Ensemble	**30.3**	**243**	**30.3**	**243**

Table S4. Comparison of the three, paleogeography, model runs which have significant gateway changes or changes in continent extent showing proxy-model SSTs discrepancy as RMSE and resulting pCO_2 scaling. SST proxies are from n=7 sites. The paleogeography estimates in this table can be compared with the ensemble mean in Table S3 for the scenarios without consideration of paleogeography changes.

	UVic	CESM_H	FOAM
RMSE (°C) Oligocene-Eocene	1.66	1.10	0.95
pCO_2 decrease (%)	19.9	30.3	23.2
pCO_2 decrease (ppmv)	139	243	169

Table S5. Inter-model temperature comparison using each model in turn as the true value ("perfect model approach") to assess model uncertainty for land surface mean air temperatures (MAT) and sea surface temperatures (SST). The "proxy sites" were used as sampling points and compared to sampling all suitable grid cells (i.e., all land/sea grid cells for MAT/SST respectively) to assess the potential reduction in uncertainty with a larger number of possible sampling locations. The RMSE and pCO_2 decrease are the mean of all other models when each model simulation is used as the true temperature values.

Model Run	MAT				SST			
	Proxy sites n=6		All land n=960		Proxy sites n=6		All marine n=710	
	RMSE (°C)	pCO_2 decrease (%)	RMSE (°C)	pCO_2 decrease (%)	RMSE (°C)	pCO_2 decrease (%)	RMSE (°C)	pCO_2 decrease (%)
CESM_B	2.80	25.6	1.65	41.3	1.39	37.7	1.32	38.9
CESM_H	1.79	34.7	1.64	41.1	1.16	41.3	1.41	36.9
GFDL CM2.1	2.56	26.4	2.04	26.4	1.74	24.4	1.94	23.9
HadCM3BL	1.50	47.4	1.83	49.3	0.80	54.3	1.50	44.7
FOAM	1.82	34.3	1.96	38.3	1.74	32.3	1.84	31.5
NorESM-L	2.14	32.0	1.77	43.4	0.95	53.6	1.12	51.2
Ensemble	**1.37**	**51.1**	**1.42**	**49.2**	**1.09**	**48.2**	**1.18**	**48.1**

Table S6. Effect of time window selection to characterize each time period (4, 2 or 1 Ma) on proxy-model MAT RMSE (°C). There is no notable improvement in the RMSE when comparing 4 Ma (time windows used in the paper) versus 2 or 1 Ma windows.

Model	4 Ma time averaging RMSE (°C)	4 Ma time averaging pCO_2 decrease (%)	2 Ma time averaging RMSE (°C)	2 Ma time averaging pCO_2 decrease (%)	1 Ma time averaging RMSE (°C)	1 Ma time averaging pCO_2 decrease (%)	ΔRMSE (2 Ma-4 Ma)	Δ RMSE (1 Ma-4 Ma)
CESM_B	2.01	18.8	2.01	19.9	2.10	21.0	0.00	0.09
CESM_H	1.68	28.3	1.78	28.3	1.58	35.8	0.10	-0.10
GFDLCM 2.1	1.38	26.3	1.38	27.3	1.64	24.2	0.00	0.26
HadCM3BL	2.23	23.2	2.34	21.0	2.18	40.1	0.11	-0.05
FOAM	1.60	29.3	1.69	29.3	1.75	31.2	0.09	0.15
NorESM-L	2.34	10.5	2.44	5.4	2.55	16.5	0.10	0.21
Ensemble	**1.88**	**30.3**	**2.04**	**29.3**	**2.08**	**40.1**	**0.16**	**0.20**

Table S7. Time interval impact on proxy-model SST comparison. Model SST RMSE (°C) from adjusted time window used for the proxies. The time windows used in this comparison include 4, 2, and 1 Ma do not have a significant difference, the 4 Ma is selected for this study.

Model	4 Ma time averaging RMSE (°C)	4 Ma time averaging pCO_2 decrease (%)	2 Ma time averaging RMSE (°C)	2 Ma time averaging pCO_2 decrease (%)	1 Ma time averaging RMSE (°C)	1 Ma time averaging pCO_2 decrease (%)	ΔRMSE (2 Ma-4 Ma)	Δ RMSE (1 Ma-4 Ma)
CESM_B	0.90	33.1	0.80	26.3	1.93	50.7	-0.10	1.03
CESM_H	0.92	35.8	0.65	29.3	1.96	48.6	-0.27	1.04
GFDLCM 2.1	1.02	21.0	0.79	17.6	2.19	32.2	-0.23	1.17
HadCM3BL	1.23	46.4	0.52	44.1	1.41	69.6	-0.71	0.18
FOAM	1.07	27.3	0.67	23.2	2.05	42.6	-0.41	0.98
NorESM-L	1.45	43.4	0.78	39.3	1.28	58.2	-0.67	-0.17
Ensemble	**1.01**	**33.1**	**0.67**	**28.3**	**1.98**	**48.6**	**-0.34**	**0.97**

Table S8. Testing the effect of excluding single MAT proxy records (n=6 reduced to n=5) on a) RMSE (°C) and b) pCO_2 decrease (%) for the pCO_2 scaling.

Model	All proxies (n=6)		Excluding the following 1 record from the proxy set: Prydz Bay bayMBT		Prydz Bay S-index		CIROS-1 /CRP S-index		WW7 BayMBT		Site 696 NLR		Site 1172 NLR	
	a	b	a	b	a	b	a	b	a	b	a	b	a	b
CESM_B	1.98	19	1.40	16	1.96	19	2.14	20	2.01	13	2.24	18	2.08	22
CESM_H	1.68	28	1.54	18	1.95	24	2.11	26	1.77	23	1.76	32	1.47	35
GDFLCm 2.1	1.35	26	1.22	19	1.51	25	1.56	28	1.38	24	1.27	30	0.95	32
HadCM3BL	2.24	23	1.80	0	2.38	9	2.57	0	2.20	7	2.44	26	2.38	31
FOAM	1.58	29	1.51	18	1.87	25	2.02	26	1.69	24	1.79	30	1.51	34
NorESM-L	2.34	11	1.80	0	2.39	0	2.57	0	2.20	0	2.57	8	2.55	13
Ensemble	**1.88**	**30**	**1.66**	**16**	**2.11**	**26**	**2.32**	**25**	**1.94**	**24**	**1.99**	**36**	**1.76**	**40**

Table S9. Effect of removing individual SST proxy records (n=6 reduced to n=5) on a) RMSE (°C) and b) pCO_2 decrease (%) for the pCO_2 scaling.

Model	All proxies (n=6)		Excluding the following 1 record from the proxy set: Prydz Bay BAYSPAR		Site 689 Δ_{47}		Site 511 BAYSPAR		Site 277 BAYSPAR		Site 277 BAYSPLINE		Site 1172 BAYSPAR	
	a	b	a	b	a	b	a	b	a	b	a	b	a	b
CESM_B	0.90	33	1.00	31	0.99	34	0.96	30	0.96	30	1.01	31	0.53	38
CESM_H	0.92	36	0.88	34	0.80	37	0.88	32	0.88	32	0.96	33	0.77	38
GDFLCm 2.1	1.02	21	0.89	21	0.87	23	0.99	20	0.99	20	1.05	20	0.85	24
HadCM3BL	1.23	46	1.07	50	0.92	55	0.76	51	0.76	51	0.85	52	0.71	58
FOAM	1.07	27	1.18	25	1.01	29	0.94	26	0.94	26	1.02	26	0.91	31
NorESM-L	1.45	43	0.92	49	0.94	51	1.18	43	1.18	43	1.28	43	1.53	46
Ensemble	**1.01**	**33**	**0.93**	**33**	**0.83**	**36**	**0.90**	**32**	**0.90**	**32**	**0.97**	**32**	**0.79**	**38**

Table S10. Impact on removing all records of the same proxy type for MAT to evaluate individual proxy impacts on the pCO_2 scaling experiment.

Model	All proxies (n=6)		bayMBT (n=4)		S-index (n=4)		NLR (n=4)	
	RMSE (°C)	pCO_2 decrease (%)	RMSE (°C)	pCO_2 decrease (%)	RMSE (°C)	pCO_2 decrease (%)	RMSE (°C)	pCO_2 decrease (%)
CESM_B	1.98	18.8	1.14	19.7	2.18	21.0	1.98	34.0
CESM_H	1.68	28.3	1.20	43.0	1.83	26.3	0.78	47.9
GDFLCM 2.1	1.35	26.3	1.03	37.8	1.56	26.3	0.63	35.8
HadCM3BL	2.24	23.2	1.29	35.7	2.01	41.0	2.65	34.0
FOAM	1.58	29.3	1.15	38.3	1.76	27.3	0.57	47.9
NorESM-L	2.34	10.5	1.29	8.7	2.07	40.1	2.85	11.7
Ensemble	**1.88**	**30.3**	**1.28**	**53.6**	**1.93**	**30.3**	**1.41**	**54.6**

Table S11. Effect of removing proxy types for MAT to evaluate individual proxy impacts on the pCO_2 scaling experiment.

Model	All proxies (n=6)		BAYSPAR (n=3)		BAYSPLINE (n=5)		Δ_{47} (n=5)	
	RMSE (°C)	pCO_2 decrease (%)	RMSE (°C)	pCO_2 decrease (%)	RMSE (°C)	pCO_2 decrease (%)	RMSE (°C)	pCO_2 decrease (%)
CESM_B	0.90	33.1	0.53	31.2	0.97	31.2	0.94	34.9
CESM_H	0.92	35.8	0.86	31.2	0.93	34.0	0.87	39.3
GDFLCM 2.1	1.02	21.0	0.89	17.6	1.05	19.9	0.93	25.3
HadCM3BL	1.23	46.4	0.59	62.1	1.22	43.4	1.34	45.7
FOAM	1.07	27.3	0.72	31.2	1.08	25.3	1.16	28.3
NorESM-L	1.45	43.4	1.48	29.3	1.34	41.0	1.36	58.2
Ensemble	**1.01**	**33.1**	**0.86**	**31.2**	**1.02**	**31.2**	**1.02**	**36.7**

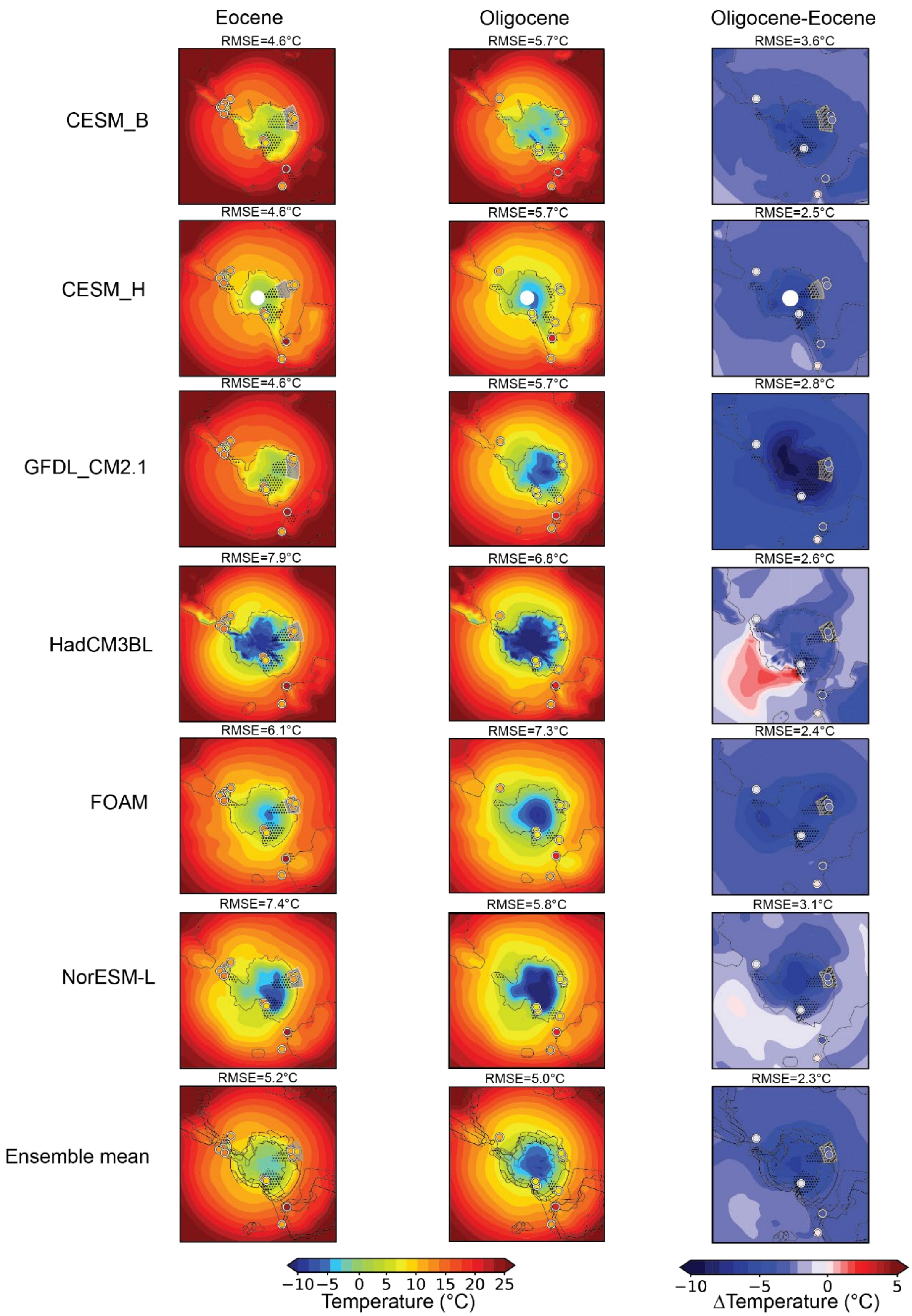

Figure S1. Southern hemisphere high latitude surface air temperatures for the Eocene (4x pCO_2 model runs), Oligocene (2x pCO_2), and the difference across the transition (2x-4x) for the various climate models and the ensemble mean. The circles correspond to proxy mean annual air temperature records while the dotted areas show the source area used to compare the model temperature to the proxy record. The grey area in the Eocene timeslice identifies the separate source regions used in Prydz Bay based on the proxy type – a larger catchment is used for the rock weathering proxy (S-index) which almost certainly has more high-altitude erosional influence, whereas a smaller catchment is used for the soil biomarker proxy (brGDGTs) as these are presumably dominated by production in lower altitudes (Tibbett et al., 2021). In the Oligocene run the catchment is restricted for Prydz Bay and the Ross Sea on the basis of ice expansion reducing the effective catchment area. In the Oligocene-Eocene panel the grey panel represent the Eocene area used for Prydz Bay while the line for source region corresponds to proxy sourcing areas for the Oligocene where an ice sheet may have reached the coast.

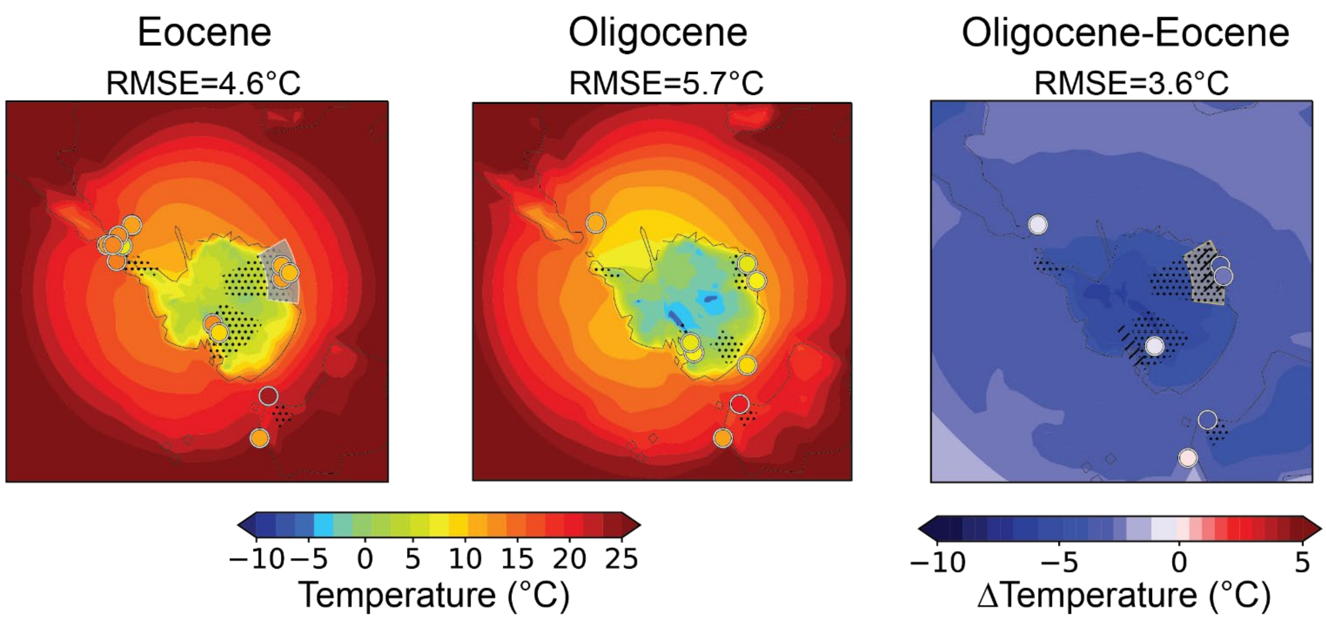

Figure S2. Zoom in from Figure S1 CESM_H simulations for source region comparisons. The grey area in the Eocene timeslice identifies the separate source regions used in Prydz Bay based on the proxy type – a larger catchment is used for the rock weathering proxy (S-index) which almost certainly has more high-altitude erosional influence, whereas a smaller catchment is used for the soil biomarker proxy (brGDGTs) as these are presumably dominated by production in lower altitudes (Tibbett et al., 2021). In the Oligocene run the catchment is restricted for Prydz Bay and the Ross Sea on the basis of ice expansion reducing the effective catchment area. In the Oligocene-Eocene panel the grey panel represents the Eocene area used for Prydz Bay while the line for source region corresponds to proxy sourcing areas for the Oligocene where an ice sheet may have reached the coast.

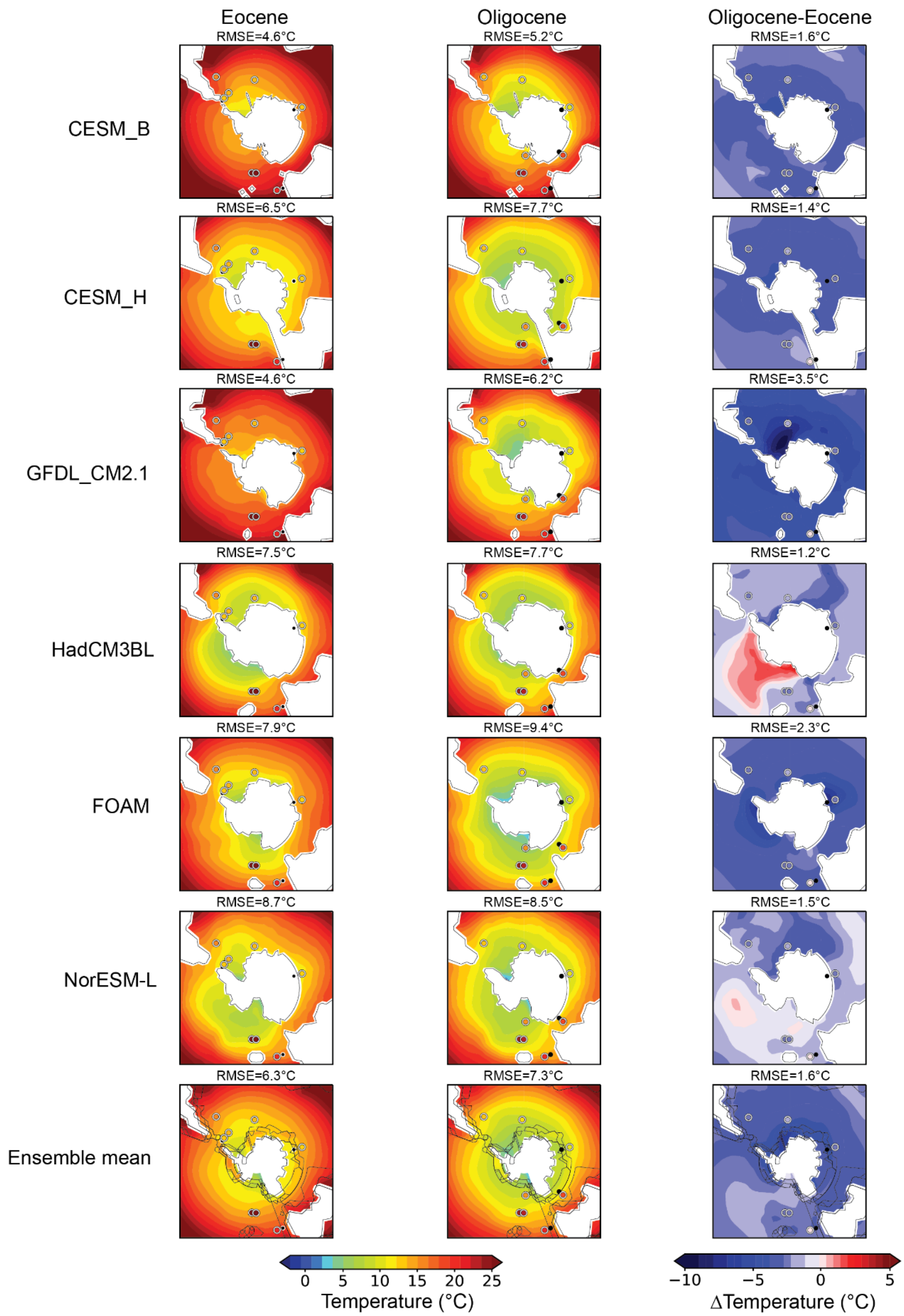

Figure S3. Modelled Southern Ocean SSTs for the Eocene (4x pCO_2 model runs), Oligocene (2x pCO_2), and the difference across the transition (2x-4x). The colored circles show proxy SSTs estimates, when these marine core sites appear to plot "on land", this is due to imprecision in modelled coastlines, and a black circle denotes the nearest marine location in the model used for proxy-model comparison.

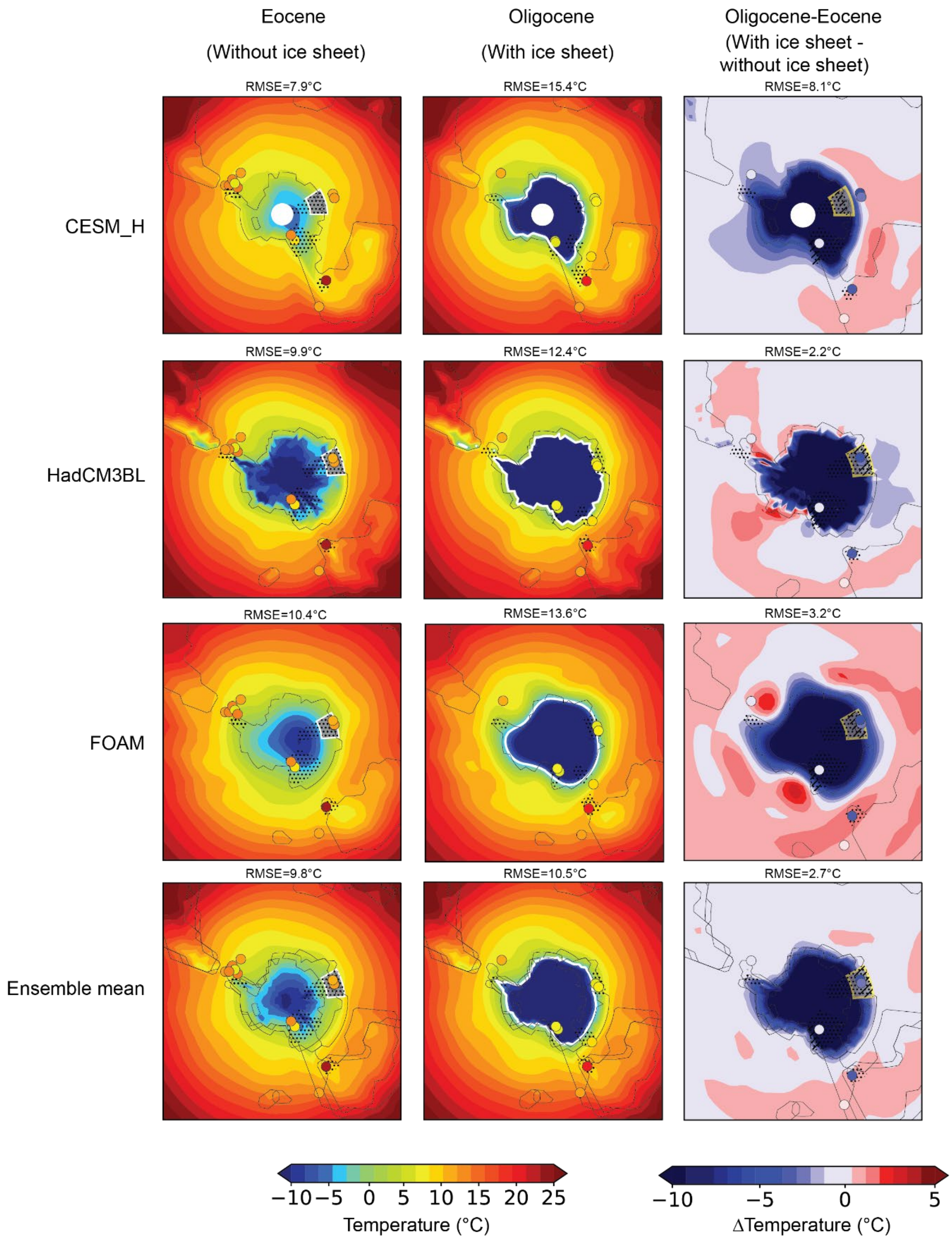

Figure S4. Climate model reconstructions for the Eocene (without ice), Oligocene (with ice) and Oligocene-Eocene showing the modelled surface air temperature (MAT) change associated with EOT glaciation. Circles show proxy evidence for MAT for comparison. White outline denotes -5°C to indicate ice sheet extent.

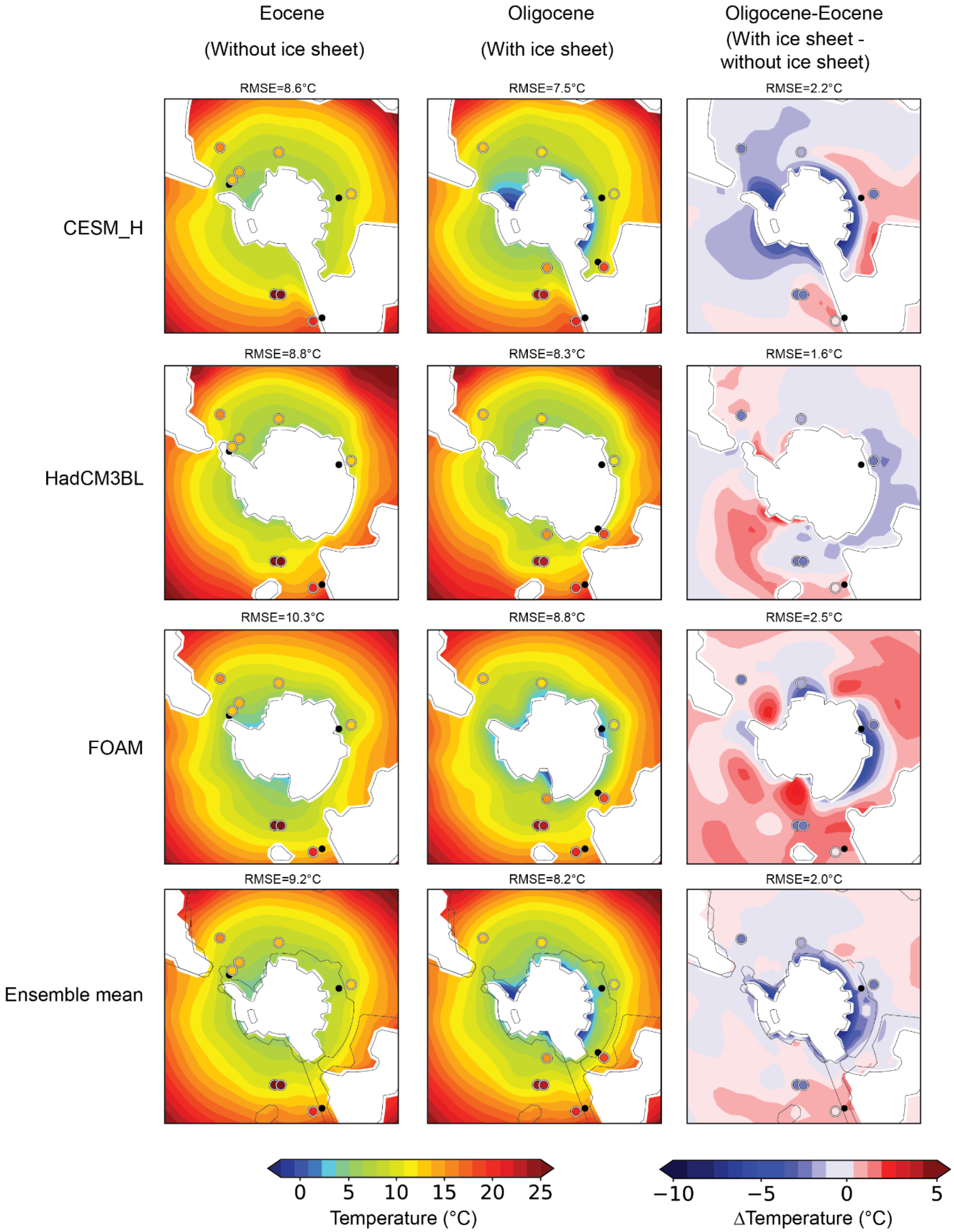

Figure S5. Climate model reconstructions for the Eocene (without ice), Oligocene (with ice) and Oligocene-Eocene showing the modelled sea surface temperature (SST) change associated with EOT glaciation. Circles show proxy evidence for SSTs for comparison.

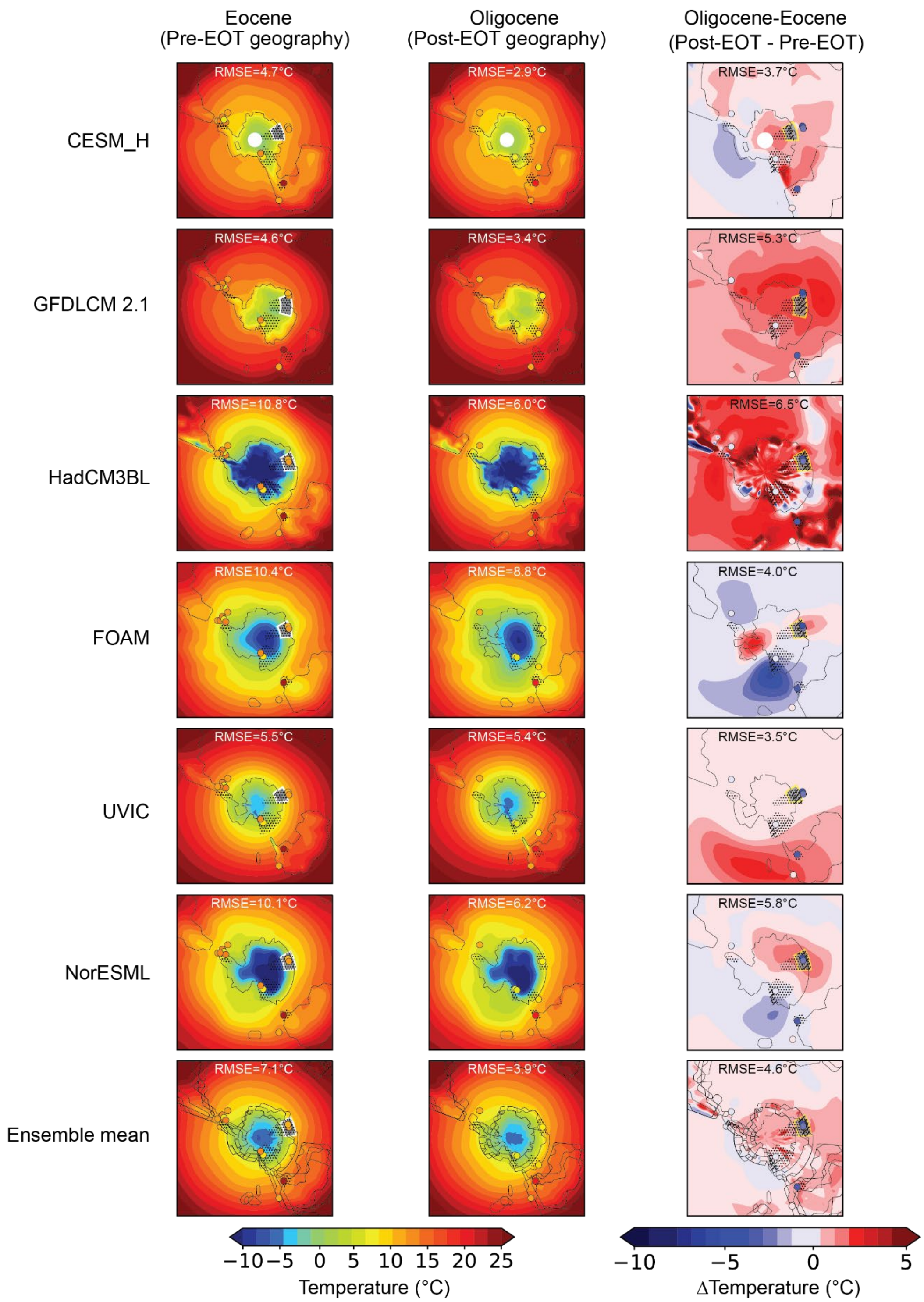

Figure S6. Climate model MAT reconstructions of Eocene, Oligocene and Oligocene-Eocene difference associated with changes in geography. CESM_H contrasts Tasman Gateway closed in the Eocene and open in the Oligocene. FOAM compares the geography of West Antarctica, being above sea level (Eocene) and below sea level (Oligocene). The UVIC experiments compare a closed (Eocene) and open (Oligocene) Drake Passage. Circles show surface air temperature values reconstructed from proxies.

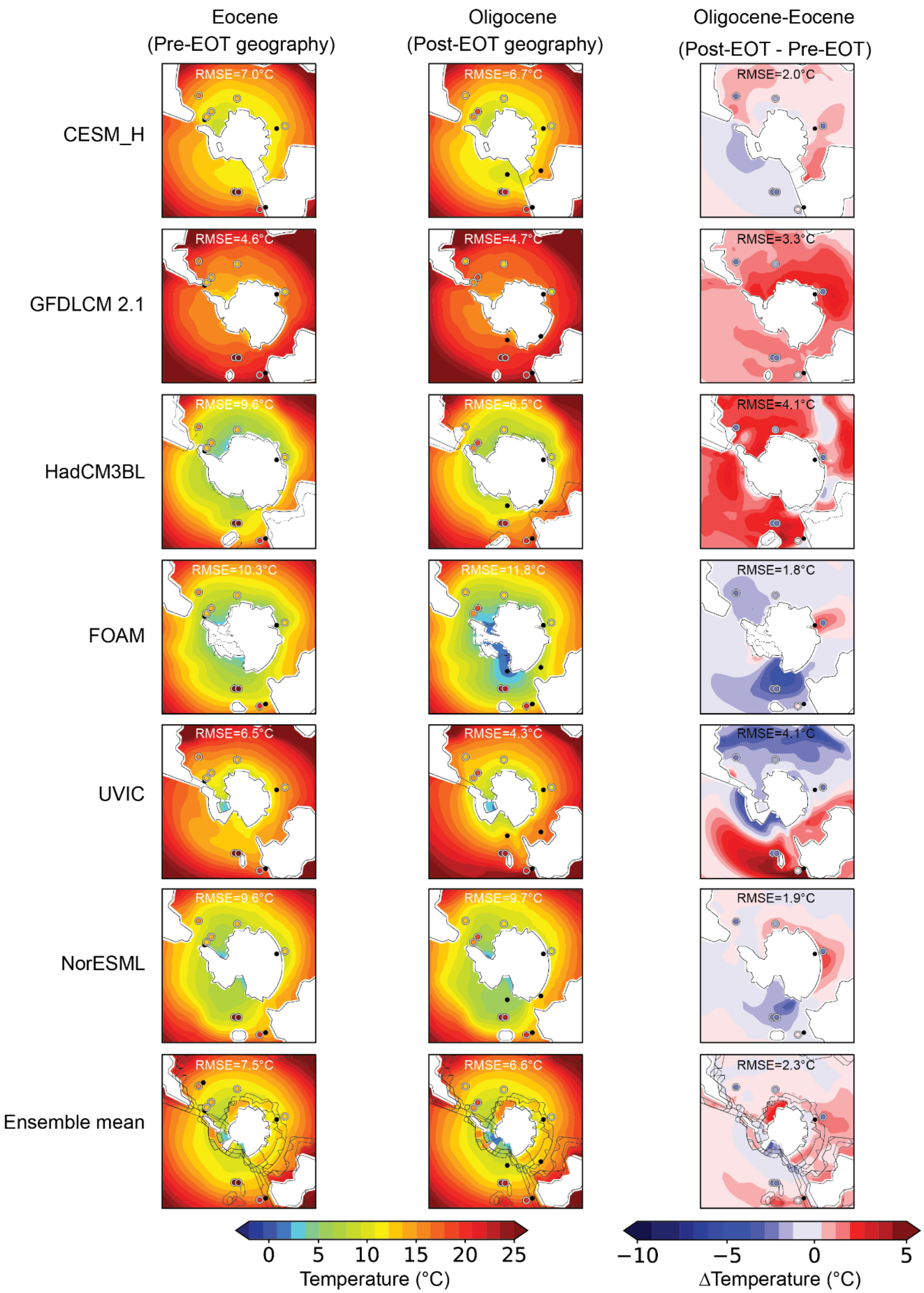

Figure S7. SST comparison between Eocene and Oligocene climate model scenarios with different paleogeographies, and proxy-model comparison. Experiments, as in Figure S3.

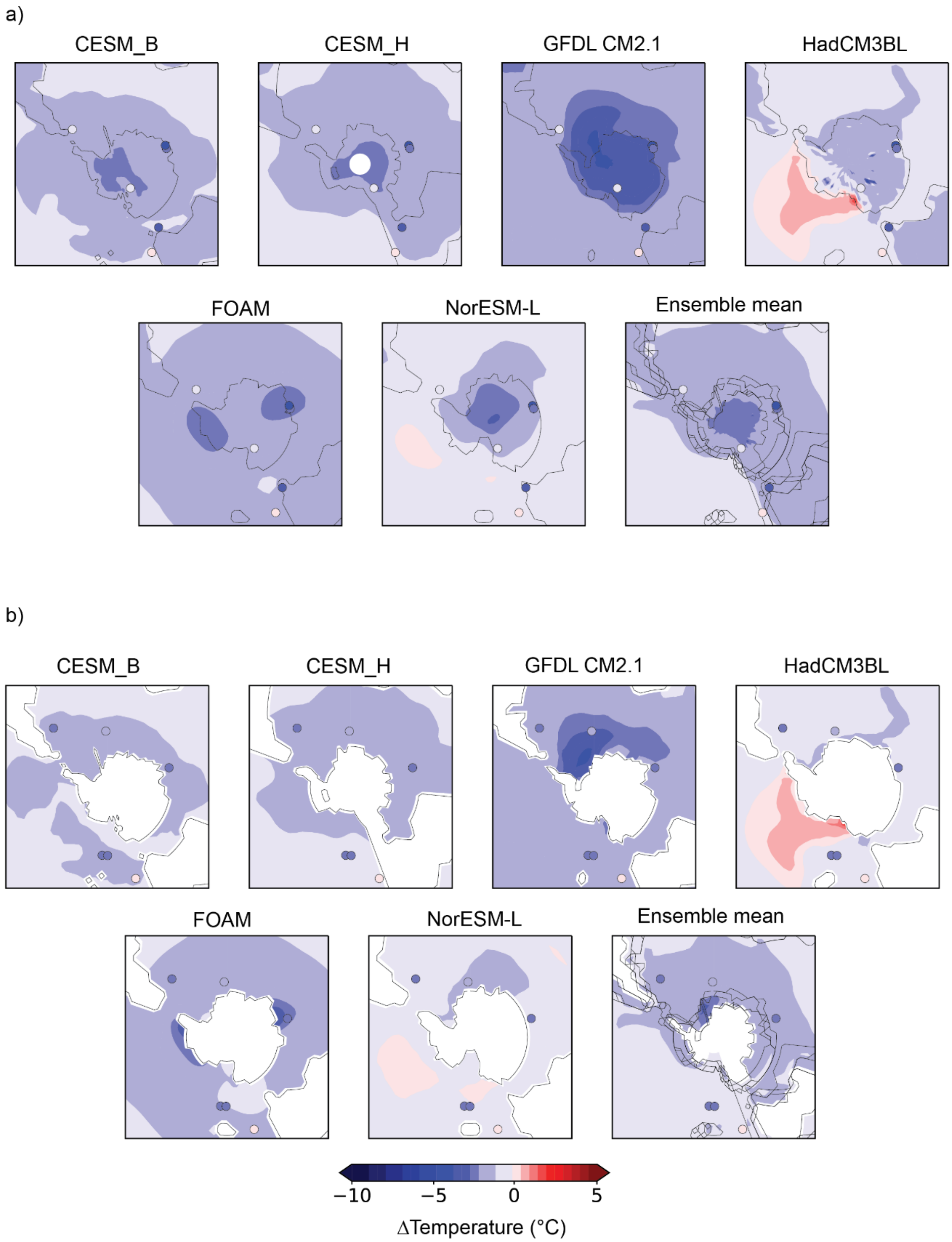

Figure S8. Proxy-model comparison for models scaled to a 25% reduction in *p*CO_2 for Oligocene-Eocene scenarios showing a) MAT b) SST. The colored circles show proxy SSTs estimates, when these marine core sites appear to plot "on land", this is due to imprecision in modelled coastlines, and a black circle denotes the nearest marine location in the model used for proxy-model comparison.

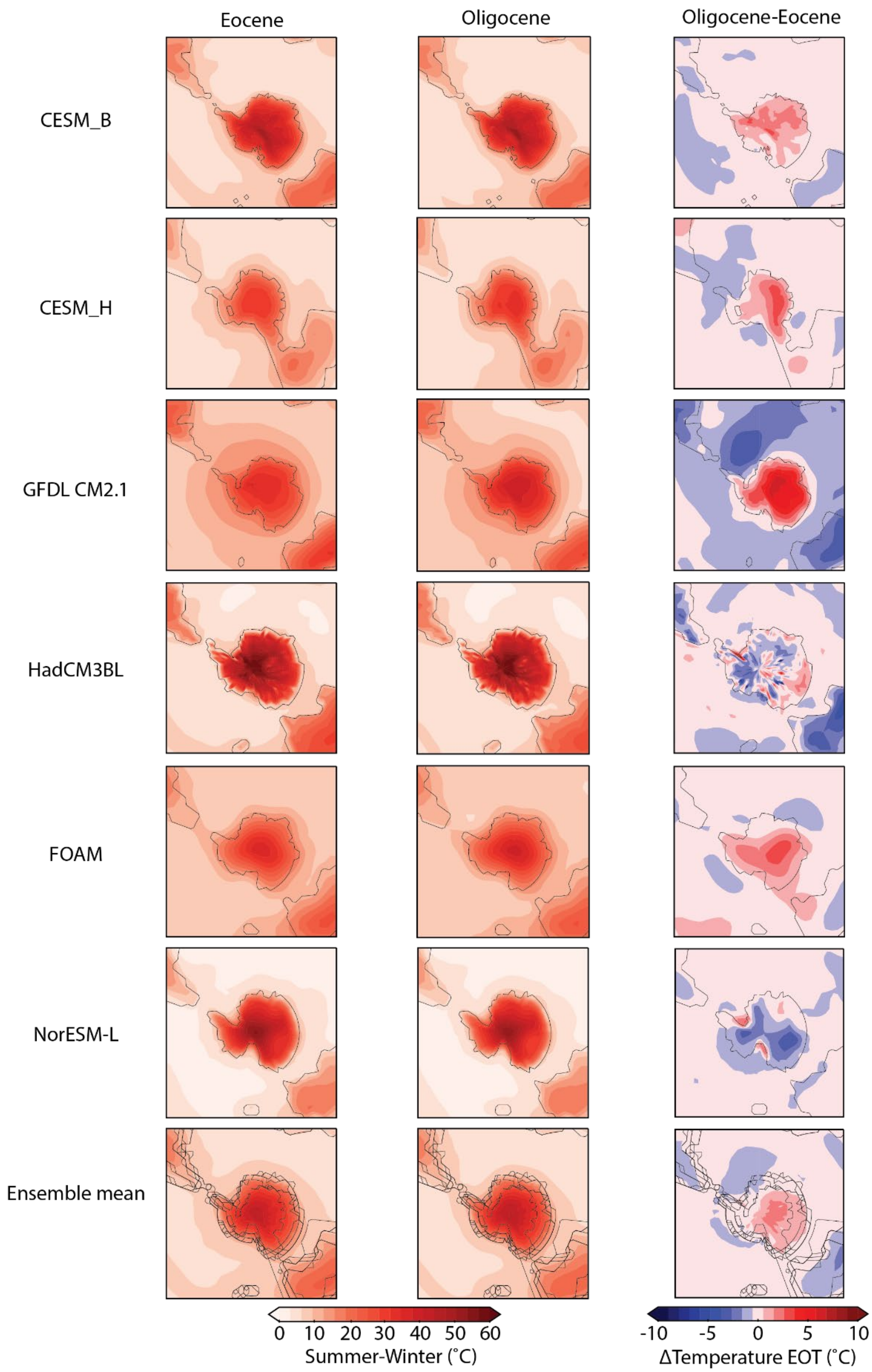

Figure S9. Model seasonality (summer-winter) for the Eocene and Oligocene timeslices and Oligocene-Eocene difference.

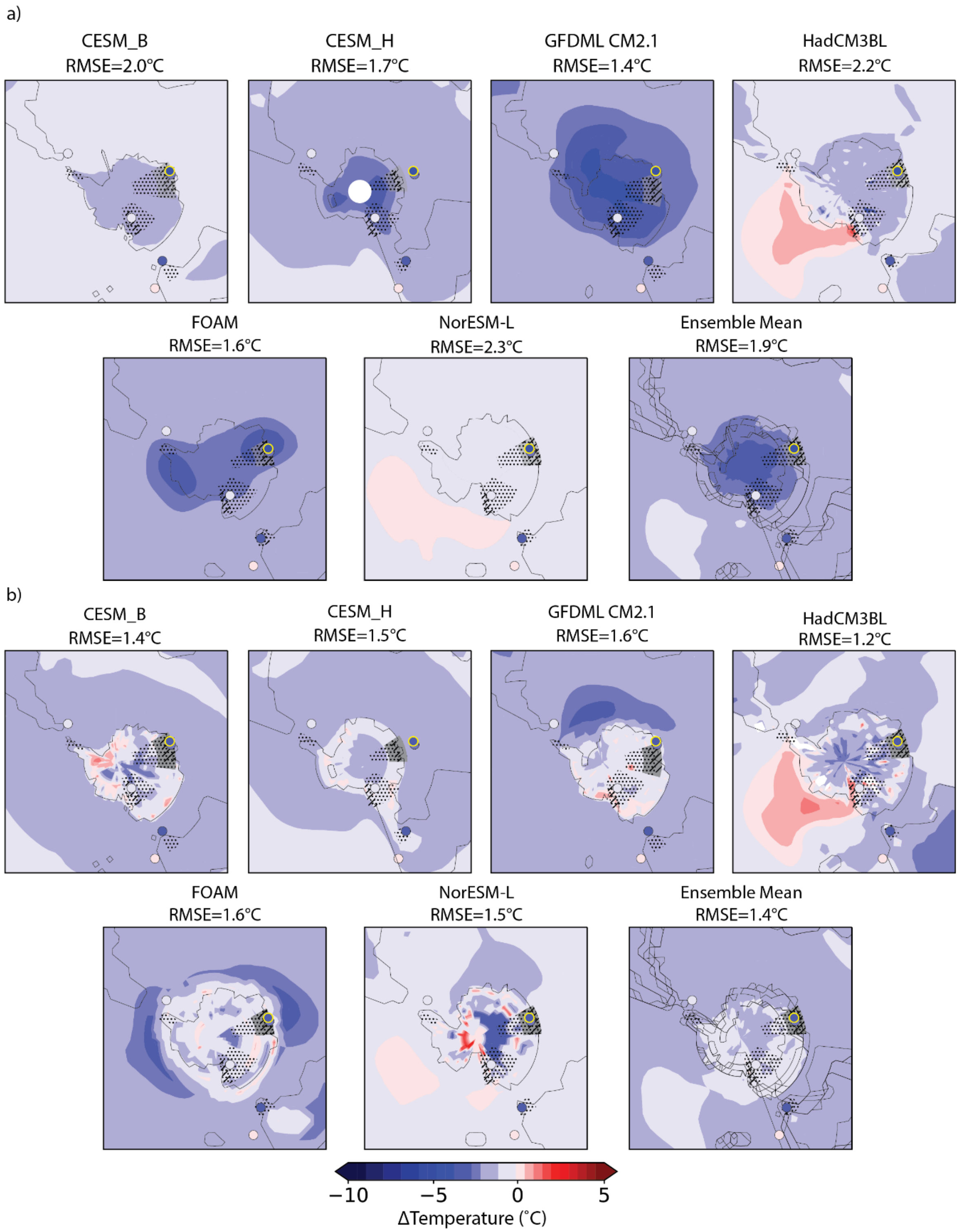

Figure S10. Best fit for pCO_2 across all models for a) MAT and b) MAF with RMSE for each model and the ensemble mean. The yellow outline marks the proxy site that was recalibrated to MAF.

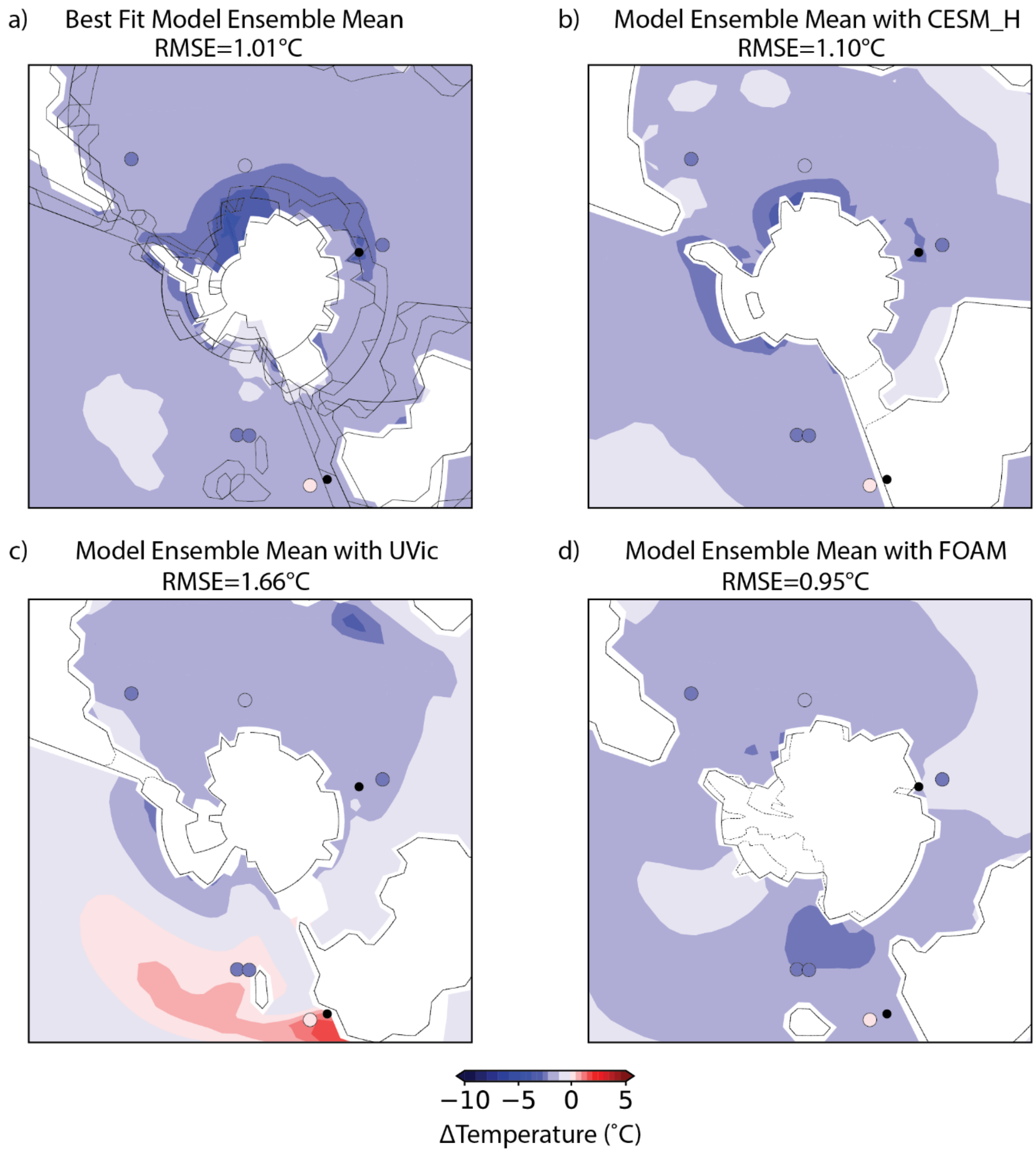

Figure S11. a) $p\mathrm{CO_2}$ best fit model ensemble mean for Oligocene-Eocene b) $p\mathrm{CO_2}$ from panel a + CESM_H ΔEOT paleogeography c) $p\mathrm{CO_2}$ from panel a + $p\mathrm{CO_2}$ from panel a + ΔEOT UVic paleogeography d) $p\mathrm{CO_2}$ + FOAM ΔEOT paleogeography.

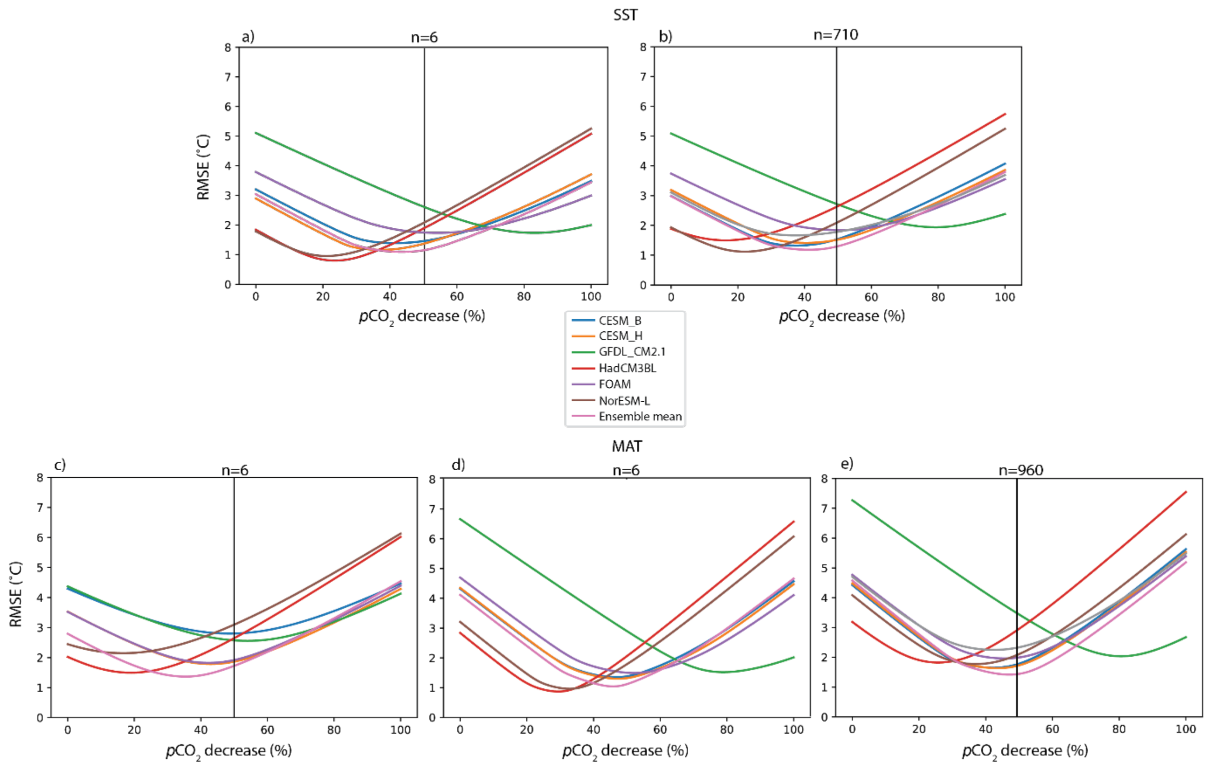

Figure S12. The "perfect model approach" assessment of inter-model temperature sensitivity to pCO_2 scaling. For each iteration one model or the ensemble mean (see legend) is used as the true temperature values ("perfect model" approach) with the additional models scaled to the "perfect mode" to assess how well the models replicate the 50% decrease in pCO_2. We show how the RMSE based on the remaining models changes across scaling factors for a) SSTs sampled at the proxy locations in the perfect model (n=6) and b) all possible marine grid cells within set parameters (n=710); c) MATs sampled at the proxy locations within the perfect model (n=6) using the adjusted source regions for the Eocene and Oligocene to account for ice sheet extent during the Oligocene, d) proxy location using the same source are for both the Eocene and Oligocene timeslices and e) then with all possible land grid cells (n=960). The black line marks the 50% decrease in pCO_2 which is the expected lowest RMSE given that a 50% decrease in pCO_2 was in fact imposed in the respective "perfect model" datasets. The RMSE does indeed minimize near 50% when the ensemble mean is used as the "prefect model" with only a slight improvement when more locations are added, indicating that the current sample size of proxy location should be adequate. The range RMSE minima in pCO_2 % decrease seen when using a given model as the "perfect model" is due to model differences in their regional climate sensitivity to the given pCO_2 change.